Transportation Research Part B 112 (2018) 89–112

Contents lists available at ScienceDirect

Transportation Research Part B

journal homepage: www.elsevier.com/locate/trb

Integrated optimization of traffic signals and vehicle trajectories at isolated urban intersections

Chunhui Yu[a,c], Yiheng Feng[b], Henry X. Liu[b,c,*], Wanjing Ma[a], Xiaoguang Yang[a]

[a] Key Laboratory of Road and Traffic Engineering of the Ministry of Education, Tongji University, 4800 Cao'an Road, Shanghai, PR China
[b] University of Michigan Transportation Research Institute (UMTRI), 2901 Baxter Rd, Ann Arbor, MI, 48109, USA
[c] Department of Civil and Environmental Engineering, University of Michigan, 2320 G.G. Brown, 2350 Hayward Street, Ann Arbor, MI, USA

ARTICLE INFO

Article history:
Received 20 July 2017
Revised 13 April 2018
Accepted 14 April 2018

Keywords:
Connected and automated vehicle
Integrated optimization
Vehicle trajectory planning
Mixed integer linear programming model
Isolated urban intersection

ABSTRACT

Existing traffic signal control systems only allocate green time to different phases to avoid conflicting vehicle movements. With advances in connected and automated vehicle (CAV) technologies, CAV trajectories not only provide more information than existing infrastructure-based detection systems, but also can be controlled to further improve mobility and sustainability. This paper presents a mixed integer linear programming (MILP) model to optimize vehicle trajectories and traffic signals in a unified framework at isolated signalized intersections in a CAV environment. A new planning horizon strategy is applied to conduct the optimization. All vehicle movements such as left-turning, right-turning and through are considered. Phase sequences, green start and duration of each phase, and cycle lengths are optimized together with vehicle lane-changing behaviors and vehicle arrival times for delay minimization. Vehicles are split into platoons and are guaranteed to pass through the intersection at desired speeds and avoid stops at stop bars. Exact vehicle trajectories are determined based on optimized vehicle arrival times. For the trajectory planning of platoon leading vehicles, an optimal control model is implemented to minimize fuel consumption/emission. For following vehicles in a platoon, Newell's car-following model is applied. Simulation results validate the advantages of the proposed control method over vehicle-actuated control in terms of intersection capacity, vehicle delays, and CO_2 emissions. A sensitivity analysis is conducted to show the potential benefits of a short minimum green duration as well as the impacts of no-changing zones on the optimality of the proposed model.

1. Introduction

With increasing traffic demand, vehicles suffer from severe traffic congestions, which cause environmental problems and economic losses (Koonce et al., 2008). Intersections are usually considered the bottlenecks for traffic flows in urban transportation networks. As reported in National Transportation Operations Coalition (NTOC) (2012), delays at traffic signals on major roadways were estimated to be 295 million vehicle-hours. Improving traffic signal operations is supposed to have a

* Corresponding author at: Department of Civil and Environmental Engineering, University of Michigan, 2320 G.G. Brown, 2350 Hayward Street, Ann Arbor, MI, USA.
E-mail addresses: 13ych@tongji.edu.cn (C. Yu), yhfeng@umich.edu (Y. Feng), henryliu@umich.edu (H.X. Liu), mawanjing@tongji.edu.cn (W. Ma), yangxg@tongji.edu.cn (X. Yang).

https://doi.org/10.1016/j.trb.2018.04.007
0191-2615/

significant impact on the efficiency of transportation systems in dense urban areas, potentially more effective than any other operational measures in the traffic engineering toolkit (NTOC, 2012).

Traditional traffic control strategies include fixed-time, vehicle-actuated, and adaptive signal control. Fixed-time control utilizes historical traffic data to calibrate pre-set signal parameters such as phase sequences, cycle lengths, and green splits. Vehicle-actuated and adaptive signal control apply infrastructure-based detectors to collect real-time traffic data and adjust signal timings according to time-variant traffic demand. Abundant studies have been dedicated to traditional signal control including stage-based (Allsop, 1981; Webster, 1958), group-based (phase-based) (Heydecker, 1992; Silcock, 1997), and lane-based approaches (Wong and Heydecker, 2011; Wong and Wong, 2003a, b). In the stage-based approach, compatible traffic movements are grouped and move together in the same time span, called a stage. Green time is then allocated to each stage. In the group-based approach, there is no need to specify a stage structure. Green time is directly allocated to each traffic movement. In the lane-based approach, signals can be optimized together with lane markings to further ameliorate traffic condition.

Thanks to the advances of connected and autonomous vehicle (CAV) technologies, communications between vehicles (V2V) and between vehicles and infrastructure (V2I) provide a new source of data for traffic control. This bilateral communication renders it possible to convey traffic information (e.g., signal timings or speed advisory) from intersections to vehicles in real time for trajectory planning as well as collect detailed vehicle trajectory data (e.g., speeds and locations) for signal control. The new technologies have the potential to prompt new opportunities for traffic control in a more effective way.

One research area tried to incorporate real-time CAV trajectory information into signal optimization, in addition to infrastructure-based detector data. Starting with a simplified two-approach intersection, Ilgin Guler et al. (2014) proposed an algorithm by combining information from CAVs and loop detectors to optimize the sequences of vehicles discharging from the intersection to minimize vehicle delays and stops. The time a CAV entered the zone of interest and the distance from the intersection were recorded to estimate virtual arrival time and queue length. Feng et al. (2015) applied the standard North American National Electrical Manufacturing Association (NEMA) dual-ring, eight-phase structure for signal optimization using CAV trajectories. The trajectory information of connected vehicles was also utilized to estimate the locations and speeds of unequipped vehicles. The phase sequence and duration within each barrier group were formulated in a two-level optimization problem. Dynamic programming (DP) was adopted to solve the problem. He et al. (2012) investigated a platoon-based arterial signal optimization model for different travel modes on the basis of real-time platoon request data and signal status. A mixed-integer linear program (MILP) was formulated to solve the problem with flexible cycle lengths and offsets. In addition to delays in the objective function, other performance metrics have also been explored such as weighted cumulative waiting time (WCWT) (Datesh et al., 2011) and cumulative travel time (CTT) (Lee and Park, 2012).

Another research area assumes that signal timings are fixed and known. Signal information is used to optimize CAV trajectories by controlling vehicle speeds or acceleration rates to reduce fuel/energy consumption, emission, delay and so on. Typically, an optimal control problem is formulated regarding locations and speeds as state variables and acceleration\deceleration as control variables (Kamal et al., 2013). However, it is generally difficult to solve an optimal control model efficiently with complex objective and constraint formulations. One direct approach is to discretize time and state space (Miyatake et al., 2011). The optimal control problem is then converted into a multistage decision process so that DP can be applied. Another effective approach is to divide a vehicle trajectory into several segments with constant acceleration/deceleration to reduce computational burden. He et al. (2015) and Wu et al. (2015) built approximation models with three trajectory segments. Vehicles were supposed to accelerate/decelerate to an optimal cruising speed; then travel at this speed; and finally accelerate/decelerate to a final speed when passing through the intersection. Therefore, the optimal control problem was transformed into a non-linear optimization problem with much fewer decision variables. Nevertheless, Wan et al. (2016) argued that the three-segment trajectory was impractical because it was uncomfortable to the occupants and potentially disruptive to the traffic. Instead, a two-segment trajectory was more implementable although it might be sub-optimal. A vehicle either accelerated with the maximum torque or decelerated with the engine off to a constant speed and then cruised past the intersection. Further, Rakha and Kamalanathsharma (2011) and Kamalanathsharma and Rakha (2013) took the downstream of an intersection, where a vehicle restored its speed, into consideration to include fuel consumption objective in the formulation. Besides analytical approaches, Wang et al. (2014a) proposed a fast numerical solution algorithm based on Pontryagin's Minimum Principle (PMP) to solve an optimal control problem for different control objectives. The algorithm was then extended to a corporative control problem (Wang et al., 2014b).

To the best of our knowledge, there are limited studies on the integrated optimization of traffic signals and vehicle trajectories in a unified framework. Malakorn and Byungkyu (2010) developed a cooperative system where a vehicle trajectory included an accelerating/decelerating segment and a cruising segment. Signals could switch dynamically between serving major and minor streets. Optimal arrival time of each vehicle was identified, which then determined the acceleration/deceleration rate within the first segment. In contrast, Li et al. (2014) assumed a generic optimal vehicle trajectory of four segments. The first and third segments had constant acceleration/deceleration rates, while the second and the fourth segments had constant speeds. Signals were optimized by enumerating all feasible signal plans. However, models of both studies were implemented at simplified intersections with two single-lane through approaches, which is unrealistic, especially in an urban traffic network. The previous signal optimization algorithms can hardly handle complex phase structures, and the optimality of trajectory segmentation was not guaranteed. Moreover, lane changing behaviors are not considered due to simplified settings of intersection geometry.

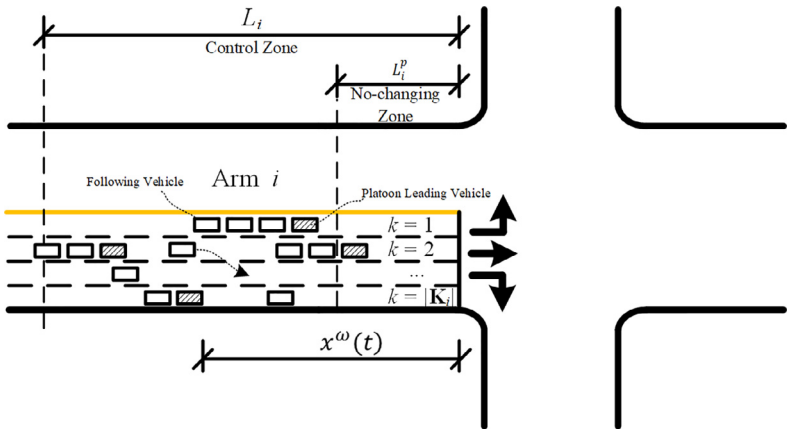

Fig. 1. An intersection with four arms.

Different from signal-based traffic control, novel "signal free" intersections were proposed where traffic signals were removed on the basis of 100% fully CAVs. Typically, vehicle trajectories are organized at an intersection by slot-based algorithms. A notable slot-based system consists of an intersection manager and vehicle agents (Dresner and Stone, 2004, 2007, 2008). An intersection is divided into a grid of several tiles which can only be occupied by one vehicle at one time. Vehicle agents send requests to the intersection manager to reserve space-time within the intersection. The intersection manager then determines whether to accept or reject the requests according to a control policy. Usually the "first come, first served" (FCFS) rule is applied. Nevertheless, vehicles are not guaranteed to avoid stops at stop bars. To improve efficiency, planning techniques were applied to optimize vehicle arrival times and speeds passing the intersection but the choice of vehicle trajectories seemed arbitrary (Au and Stone, 2010). Further, a batch strategy with adaptive vehicle platooning was developed for high traffic demand (Tachet et al., 2016). Actually, the slot-based control focuses on vehicle management within an intersection area and does not consider vehicle trajectories before arrival of the intersection. For example, vehicle trajectories are assumed to be fixed to track reservation distance. In essence, the slot-based control does not ensure the optimality in terms of vehicle platooning.

To address these research deficiencies, this paper presents an MILP model to optimize traffic signals and vehicle trajectories at isolated urban intersections in a unified framework. Phase sequences, green start and duration of each phase, and cycle lengths are optimized together with vehicle lane-changing behaviors and vehicle arrival times in the MILP model. Vehicles are guaranteed to pass through an intersection at desired speeds and avoid stops at stop bars. A new planning horizon strategy is applied to conduct the optimization. Platoons in each lane are identified based on the optimization results. Exact vehicle trajectories are then generated by optimal control models and car-following models. The trajectory of each platoon leading vehicle is optimized by an optimal control model with the objective to minimize fuel consumption and emission. Lower and upper bounds of arrival time constraints are imposed to the MILP model in order to generate feasible trajectories. Clearance time is considered to eliminate conflictions between incompatible vehicle movements within an intersection area. The proposed MILP model is similar with slot-based "signal free" models if the minimum green time constraint is removed. However, the proposed model optimizes vehicle trajectories at the upstream of an intersection instead of managing trajectories within an intersection area.

The remainder of this paper is structured as follows. Section 2 presents the problem and the key notations. Section 3 generates the trajectories of vehicles by lane based on vehicle arrival times at stop bars as well as provides arrival time constraints for the MILP model. In this way, the trajectory generation of vehicles in one lane is equivalent to the determination of arrival times. Section 4 introduces the MILP model in detail that optimize signals, vehicle arrival times, and vehicle lane choices. Section 5 conducts numerical studies and sensitivity analysis. Finally, conclusions and recommendations are delivered in Section 6.

2. Notations and problem description

2.1. Notations

Before presenting the model, two types of notations including parameters and control variables are introduced.

2.1.1. Parameters

Several types of parameters are defined in this section including geometric parameters, traffic parameters, vehicle trajectory parameters, and signal parameters. The geometric parameters which are based on the layout of an intersection are assumed to be given. Fig. 1 shows the details of one arm of a typical four-arm intersection as an example. Vehicle trajectories and signals are updated each time optimization is conducted, denoted as time t_0. Vehicles that pass a stop bar in

Table 1
Notations and parameters.

General notations	
i:	Arm index
k:	Approach lane index in each arm
(i, j):	Traffic flow from arm i to arm j, which is also called phase
ω:	Vehicle index
t_0:	Time when an optimization process starts, s
M:	A sufficiently big number
Geometrical parameters	
$\mathbf{I}$:	Set of arms at the intersection
$\zeta_k^{i,j}$:	1, if lane k in arm i is used by traffic flow (i, j); 0, otherwise
L_i:	Control zone in arm i in which vehicle trajectories are to be controlled, m
L_i^p:	No-changing zone in arm i in which vehicles keep their previously optimized trajectories, m
$\mathbf{K}_i$:	Set of approach lanes in arm i; $\mathbf{K}_i = \{1, \ldots, |\mathbf{K}_i|\}$, where $|\mathbf{K}_i|$ is the size of $\mathbf{K}_i$
$\mathbf{K}_\omega$:	Set of permitted lanes for vehicle ω, which are the dedicated lanes for the movement direction of vehicle ω
$\mathbf{K}_0$:	Set of lanes used by traffic flows having right of way at time t_0, $\mathbf{K}_0 = \{k \mid \zeta_k^{i,j} = 1, k \in \mathbf{K}_i, (i, j) \in \mathbf{\Psi}_0\}$
Traffic parameters	
$\mathbf{\Psi}$:	Set of all traffic flows at the intersection
$\mathbf{\Psi}_{ic}$:	Set of incompatible traffic flow pairs that cannot have right of way at the same time
$\mathbf{\Psi}_0$:	Set of compatible traffic flows that are receiving green at time t_0
$\mathbf{\Psi}_p$:	Set of the traffic flows whose green ended before time t_0
$\mathbf{\Omega}_i$:	Set of vehicles in arm i at time t_0
$\mathbf{\Omega}_i^p$:	Set of vehicles in the no-changing zone in arm i at time t_0, $\mathbf{\Omega}_i^p \subset \mathbf{\Omega}_i$
$\mathbf{\Omega}_\omega$:	Set of vehicles ahead of vehicle $\omega \in \mathbf{\Omega}_i$ at time t_0, whose permitted lane set overlaps with that of ω; that is, $\mathbf{\Omega}_\omega = \{\omega' \mid \mathbf{K}_{\omega'} \cap \mathbf{K}_\omega \neq \emptyset, x_0^{\omega'} < x_0^\omega, \omega' \in \mathbf{\Omega}_i\}$
Vehicle trajectory parameters	
x_0^ω:	Distance between vehicle ω and its ahead stop bar at time t_0, m
v_0^ω:	Speed of vehicle ω at time t_0, m/s
δ'^ω_k:	1, if vehicle ω is in lane k at time t_0; 0, otherwise
t'^ω_f:	Previously optimized arrival time of vehicle ω, s
t_e^ω:	Generating time of vehicle ω, s
t_l^ω:	Time of the previous lane changing behavior of vehicle ω, s
Δt_l^{min}:	Minimum time interval between two lane changing behaviors of a vehicle, s
v_f^ω:	Desired speed of vehicle ω passing through the intersection, m/s
v_{max}:	Speed limit, m/s
τ^ω:	Time displacement of vehicle ω in Newell's car-following model, s
d^ω:	Space displacement of vehicle ω in Newell's car-following model, m
a_L:	Absolute value of the maximum comfortable deceleration rate, m/s^2
a_U:	Value of the maximum comfortable acceleration rate, m/s^2
α_1:	Weight of total vehicle delay in the objective
Signal parameters	
N:	Number of signal cycles in the signal optimization horizon
Δd:	Tolerance of solution quality degradation, s
α_2:	Weight of cycle lengths in the objective
t_s:	Start time of the signal optimization horizon, s
$\theta_{i,j}^p$:	Green start for inactive traffic flow $(i, j) \in \mathbf{\Psi}_p$ in the current/first cycle. Inactive flow means the green time for this traffic flow was already terminated by time t_0, s
$\phi_{i,j}^p$:	Green duration for inactive traffic flow $(i, j) \in \mathbf{\Psi}_p$ in the current/first cycle, s
$\theta_{i,j}^0$:	Green start for active traffic flow $(i, j) \in \mathbf{\Psi}_0$ in the current/first cycle, s
$g_{min}^{i,j}$:	Minimum green duration for traffic flow (i, j), s
$\pi_{i,j,\,l,\,m}$:	Clearance time between incompatible traffic flows, defined as the earliest time when traffic flow (l, m) has right of way after traffic flow (i, j) terminates, s
$z_{i,j,l,m}^{n,s}$:	Relative time between green starts measured from traffic flow (i, j) to (l, m) in n^{th} cycle, s
$z_{i,j,l,m}^{n,e}$:	Relative time between green ends measured from traffic flow (i, j) to (l, m) in n^{th} cycle, s

the same lane in the same cycle are regarded as one platoon. The first vehicle in a platoon is the leading vehicle and the remaining vehicles in the same platoon are following vehicles. Main parameters are summarized in Table 1.

2.1.2. Control variables

Two types of control variables are defined. Let $\boldsymbol{V} = (\boldsymbol{T}, \boldsymbol{S})$ be the set of all variables, where $\boldsymbol{T}$ is the subset of vehicle trajectory variables; and $\boldsymbol{S}$ is the subset of signal variables. The control variables are updated after each optimization process. Main control variables are summarized in Table 2.

Table 2
Control variables.

Vehicle trajectory variables	
δ_k^ω:	1, if vehicle ω is in lane k; 0, otherwise
λ^ω:	1, if vehicle ω maintains its previously optimized trajectory; 0, otherwise
γ^ω:	0, if the trajectory of vehicle ω is not affected by its all preceding vehicles and is to be updated; 1, otherwise
μ^ω:	0, if vehicle ω decides to change lanes; 1, otherwise
$\eta^{\omega,\omega'}$:	0, if vehicles ω and ω' are in the same lane; 1, otherwise
$x^\omega(t)$:	Distance between vehicle ω and the ahead stop bar at time t, m
$l^\omega(t)$:	Travelled distance by vehicle ω from time t_0 to t, m
$v^\omega(t)$:	Speed of vehicle ω at time t, m/s
$a^\omega(t)$:	Acceleration/deceleration rate of vehicle ω at time t, m/s^2
t_f^ω:	Arrival time of vehicle ω at the intersection, s
Δt^ω:	Travel time of vehicle ω, s
β_n^ω:	1, if vehicle ω passes through the intersection in n^{th} cycle; 0, otherwise
Signal variables	
$\theta_{i,j}^n$:	Green start for traffic flow (i, j) in n^{th} cycle, s
$\phi_{i,j}^n$:	Green duration for traffic flow (i, j) in n^{th} cycle, s
$\Theta_{i,k}^n$:	Green start in lane k of arm i in n^{th} cycle, s
$\Phi_{i,k}^n$:	Green duration in lane k of arm i in n^{th} cycle, s
$\Lambda_{i,j,l,m}^n$:	1, if the green start of traffic flow (l, m) immediately follows that of traffic flow (i, j) in n^{th} cycle; 0, otherwise
C^n:	Cycle length of n^{th} cycle, s

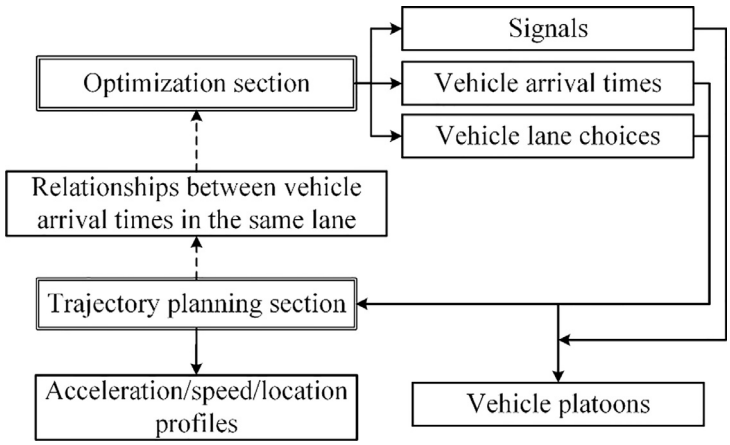

Fig. 2. Model framework.

2.2. Problem description

For a typical intersection, there are three vehicle movements (i.e., left-tuning, through, and right-turning) in each arm. Each movement has a different desired speed to pass through the intersection for safety concerns. As shown in Fig. 1, in each arm, the approach lane index is incremented from the left most lane. Each approach lane is dedicated to one vehicle movement. The distance between a vehicle and the stop bar at time t is denoted as $x^\omega(t)$. L_i is the control zone in arm i in which vehicle trajectories can be optimized. L_i^p is the no-changing zone in which vehicles keep their previously optimized trajectories. That is, only the trajectories of vehicles that are outside the no-changing zone will be updated over time. The no-changing zone is designed to reduce computational burden but at the cost of optimality.

The task is to integrate vehicle trajectory planning into traffic signal optimization in a unified framework to minimize vehicle delays. The model framework is shown in Fig. 2. The trajectory planning serves for two purposes: 1) build the relationships between vehicle arrival times in the same lane, which helps build the arrival time constraints (e.g., upper and lower bounds) in the MILP model; 2) generate trajectories for vehicles in the same lane given their arrival times, which are supposed to be optimized in the MILP model. Note that no exact vehicle trajectories or platooning are needed in building the constraints of arrival times in the MILP model. The outputs of the optimization model include signals, vehicle lane choices, and vehicle arrival times. Platoons, i.e., the vehicles that pass the stop bar in the same lane in the same cycle, are identified based on the optimization results. However, only vehicle lane choices and vehicle arrival times are needed in planning exact trajectories (i.e., acceleration, speed, and location profiles) for vehicles in each lane. Platooning is not necessarily needed when generating exact vehicle trajectories.

3. Vehicle trajectory planning

This section builds the relationships between arrival times and trajectories for vehicles in the same lane. An optimal control model is introduced to generate optimal trajectories for platoon leading vehicles with the objective of minimizing fuel consumption/emission given arrival times. The Newell's car-following models are used to capture the trajectories of following vehicles. In this way, the identification of vehicle trajectories is equivalent to determining the arrival times. To guarantee the feasibility of the optimal control models, this section also helps build the constraints of vehicle arrival times for the MILP model.

3.1. Trajectories of platoon leading vehicles

Vehicles that pass through an intersection in the same lane in the same cycle are regarded as one platoon. The first vehicle in a platoon is a platoon leading vehicle. Its trajectory is planned with the objective of reducing fuel consumption/emission. The initial state at time t_0 and the final state at the intersection (i.e., location and speed) of each platoon leading vehicle ω are known. The trajectory control strategy of vehicle ω is formulated as the solution to the following optimal control problem (**P1**). An optimal trajectory can be identified given the value of vehicle arrival time t_f^ω. It should be bounded to guarantee the feasibility of **P1**.

P1:

$$\min_{a^\omega(t)} \int_{t_0}^{t_f^\omega} |a^\omega(t)|dt \tag{1}$$

$$\begin{cases} \dot{l}^\omega(t) = v^\omega(t) \\ \dot{v}^\omega(t) = a^\omega(t) \end{cases} \tag{2}$$

$$\begin{cases} l^\omega(t_0) = 0 \\ v^\omega(t_0) = v_0^\omega \end{cases} \tag{3}$$

$$\begin{cases} l^\omega\left(t_f^\omega\right) = x_0^\omega \\ v^\omega\left(t_f^\omega\right) = v_f^\omega \end{cases} \tag{4}$$

$$0 \le v^\omega(t) \le v_{max},\ t_0 \le t \le t_f^\omega \tag{5}$$

$$\begin{aligned} &-a_L \le a^\omega(t) \le a_U,\ t_0 \le t \le t_f^\omega \\ &t_f^\omega \text{ fixed} \end{aligned} \tag{6}$$

where $l^\omega(t)$ is the distance travelled by vehicle ω from time t_0 to time t. It is different from $x^\omega(t)$ that is the distance between vehicle ω and the stop bar at time t. The integration over the absolute value of the acceleration rate is used as the objective function in Eq. (1) for fuel consumption/emission minimization. Although fuel consumption/emission may be related to both vehicle speeds and acceleration rates (Jiang et al., 2017; Wang et al., 2014a), Eq. (1) is used for simplification, which is a common practice in optimal control theory Naidu, 2002). The use of this simplified objective function has also been validated in Feng et al. (2018). Eq. (2) describes vehicle dynamics. Eqs. (3) and ((4) are the constraints of initial and final vehicle states. Eqs. (5) and (6) are the bounds of vehicle speeds and acceleration rates. The solution to **P1** is the acceleration profile of leading vehicle ω.

Eq. (5) is the constraint of a state variable (i.e., vehicle speed) in **P1**, which makes the optimal control problem difficult to solve. To address the problem, we classify the condition into two cases depending on whether the upper bound v_{max} in Eq. (5) will be violated. Fig. 3 shows the trajectories in the two cases with minimum travel time. The possible maximum speed in Fig. 3 is obtained by accelerating from the initial state $(0, v_0^\omega)$ and decelerating to the final state (x_0^ω, v_f^ω). In Fig. 3(a), the constraint Eq. (5) is never violated and it can be removed from the optimal control problem (P1). In Fig. 3(b), the constraint Eq. (5) may be active and then a trajectory segment of cruising is included.

Case 1:

If the following condition is true, then the constraint on the upper bound of speed v_{max} in Eq. (5) can be released. That means in the generated vehicle trajectory, the vehicle speed never reaches v_{max}.

$$\frac{(v_{max})^2 - \left(v_0^\omega\right)^2}{2a_U} + \frac{(v_{max})^2 - \left(v_f^\omega\right)^2}{2a_L} > x_0^\omega \tag{7}$$

A simplified optimal control problem can be solved analytically. Only the final solutions are shown here. The readers can refer to Feng et al. (2018) for detailed derivation.

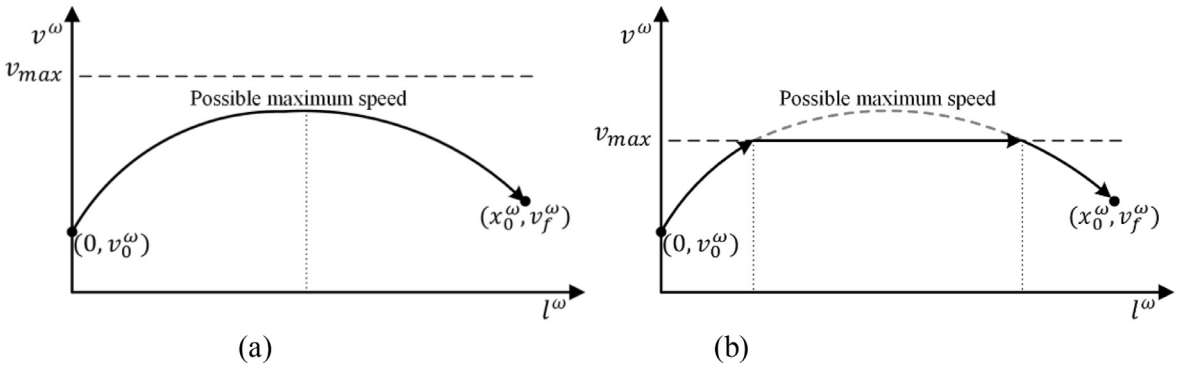

Fig. 3. Illustration of two cases: (a) Case 1, and (b) Case 2.

Denote $v_{a_L}^\omega$ and $v_{a_U}^\omega$ to be the lower and upper of vehicle speeds when the vehicle enters the control zone in each arm as

$$v_{a_L}^\omega = \sqrt{2a_L x_0^\omega + \left(v_f^\omega\right)^2} \tag{8}$$

$$v_{a_U}^\omega = \begin{cases} \sqrt{\left(v_f^\omega\right)^2 - 2a_U x_0^\omega}, & \text{if } x_0^\omega \le \frac{\left(v_f^\omega\right)^2}{2a_U} \\ 0, & \text{otherwise} \end{cases} \tag{9}$$

Vehicle ω is controllable when $v_{a_L}^\omega \ge v_0^\omega \ge v_{a_U}^\omega$ which is supposed to be satisfied. According to the proposed control strategy, vehicle ω will maintain controllable until arriving at the intersection.

Denote Δt_L^ω and Δt_U^ω as

$$\Delta t_L^\omega = \frac{v_1 - v_0^\omega}{a_U} + \frac{v_1 - v_f^\omega}{a_L} \left(v_1 = \sqrt{\frac{2a_U a_L x_0^\omega + a_L\left(v_0^\omega\right)^2 + a_U\left(v_f^\omega\right)^2}{a_L + a_U}} \right) \tag{10}$$

$$\Delta t_U^\omega = \begin{cases} +\infty, \text{ if } x_0^\omega > \frac{\left(v_f^\omega\right)^2}{2a_U} \text{ and } v_0^\omega < \sqrt{2x_0^\omega a_L - \frac{\left(v_f^\omega\right)^2 a_L}{a_U}} \\ \dfrac{v_0^\omega - v_1}{a_L} + \dfrac{v_f^\omega - v_1}{a_U} \left(v_1 = \sqrt{\frac{a_U\left(v_0^\omega\right)^2 + a_L\left(v_f^\omega\right)^2 - 2a_U a_L x_0^\omega}{a_L + a_U}} \right), \text{otherwise} \end{cases} \tag{11}$$

where Δt_L^ω and Δt_U^ω are the lower and upper bounds of travel times to reach the intersection to make **P1** feasible considering vehicle dynamics limits (refer to Feng et al. (2018) for detailed derivation). Note that $v_{a_U}^\omega$ and Δt_U^ω are piecewise functions due to the constraint $v^\omega(t) \ge 0$ in Eq. (5). Therefore, travel time Δt^ω of the leading vehicle ω can vary within the following bounds:

$$\Delta t_L^\omega \le \Delta t^\omega \le \Delta t_U^\omega \tag{12}$$

The corresponding lower and upper bound of vehicle arrival times at the intersection are thus further specified as

$$t_0 + \Delta t_L^\omega \le t_f^\omega = t_0 + \Delta t^\omega \le t_0 + \Delta t_U^\omega \tag{13}$$

The optimal trajectory of a leading vehicle is determined when Δt^ω or t_f^ω is identified (refer to Appendix A for details).

Case 2:

If the following condition holds, then the upper bound speed v_{max} may be reached in the generated trajectory:

$$\frac{(v_{max})^2 - \left(v_0^\omega\right)^2}{2a_U} + \frac{(v_{max})^2 - \left(v_f^\omega\right)^2}{2a_L} \le x_0^\omega \tag{14}$$

The difference between Case 2 and Case 1 is the calculation of the minimum travel time, denoted as $\Delta t'^\omega_L$ instead:

$$\Delta t'^\omega_L = \Delta t_1 + \Delta t_2 + \Delta t_3 \tag{15}$$

where

$$\Delta t_1 = \frac{v_{max} - v_0^\omega}{a_U} \tag{16}$$

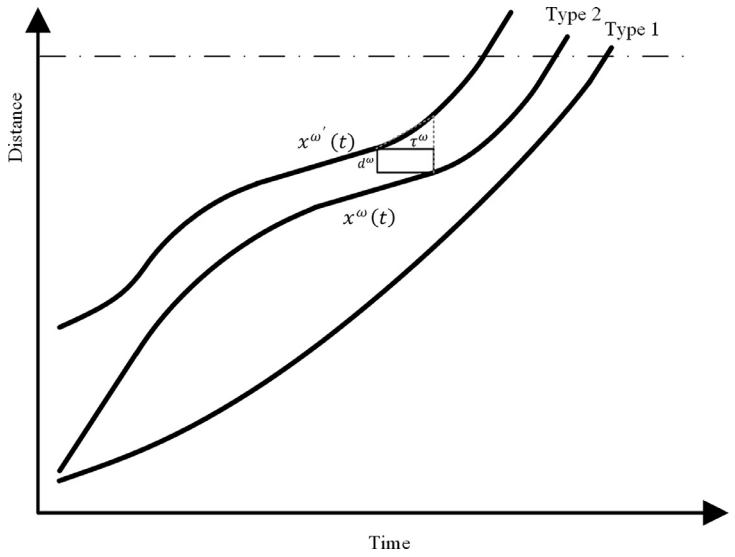

Fig. 4. Possible trajectories of a following vehicle.

$$\Delta t_2 = \frac{v_{max} - v_f^{\omega}}{a_L} \tag{17}$$

$$\Delta t_3 = \frac{x_0^{\omega} - \frac{(v_{max})^2 - (v_0^{\omega})^2}{2a_U} - \frac{(v_{max})^2 - (v_f^{\omega})^2}{2a_L}}{v_{max}} \tag{18}$$

Eq. (16) is the acceleration time from speed v_0^{ω} to v_{max} with the maximum acceleration rate a_U. Eq. (17) is the deceleration time from speed v_{max} to v_f^{ω} with the maximum deceleration rate a_L. Eq. (18) is the cruising time at speed v_{max}. Therefore, the travel time Δt^{ω} of leading vehicle ω in Case 2 is bounded by

$$\Delta t'^{\omega}_L \le \Delta t^{\omega} \le \Delta t_U^{\omega} \tag{19}$$

where Δt_U^{ω} is calculated in Eq. (11) in Case 1. The arrival time is thus bounded by:

$$t_0 + \Delta t'^{\omega}_L \le t_f^{\omega} = t_0 + \Delta t^{\omega} \le t_0 + \Delta t_U^{\omega} \tag{20}$$

The optimal trajectory can also be generated according to Appendix A when Δt^{ω} or t_f^{ω} is determined.

3.2. Trajectories of following vehicles

Generally, a following vehicle has two types of trajectories as shown in Fig. 4. If following vehicle ω is far away from its preceding vehicle ω', its trajectory is not affected by its preceding vehicle (Type 1). Otherwise, the trajectory is presented in Type 2, which is modeled by a car-following model, when following vehicle ω catches up with its preceding vehicle ω'.

Case 1: Trajectory Type 1

If vehicle ω follows trajectory Type 1, it is supposed to drive as fast as possible to minimize the delay. The trajectory is the solution of the following optimal control problem:

P2:

$$\min_{a^{\omega}(t)} \int_{t_0}^{t_f^{\omega}} 1dt = t_f^{\omega} - t_0 \tag{21}$$

$$\begin{cases} \dot{l}^{\omega}(t) = v^{\omega}(t) \\ \dot{v}^{\omega}(t) = a^{\omega}(t) \end{cases} \tag{22}$$

$$\begin{cases} l^{\omega}(t_0) = 0 \\ v^{\omega}(t_0) = v_0^{\omega} \end{cases} \tag{23}$$

$$\begin{cases} l^{\omega}\left(t_f^{\omega}\right) = x_0^{\omega} \\ v^{\omega}\left(t_f^{\omega}\right) = v_f^{\omega} \end{cases} \tag{24}$$

$$0 \le v^{\omega}(t) \le v_{max},\ t_0 \le t \le t_f^{\omega} \tag{25}$$

$$\begin{aligned} &-a_L \le a^{\omega}(t) \le a_U, t_0 \le t \le t_f^{\omega} \\ &t_f^{\omega} \text{ fixed} \end{aligned} \tag{26}$$

The constraints of **P2** are the same as those of **P1**. The objective Eq. (21) is the minimization of the travel time (i.e., delay). Actually, the solution to **P2** is a special case of **P1** in which the given arrival time t_f^{ω} is the lower bound. Therefore, the optimal travel time Δt^{ω} can be expressed as

$$\Delta t^{\omega} = \begin{cases} \Delta t_L^{\omega}, & \text{if } \frac{(v_{max})^2 - (v_0^{\omega})^2}{2a_U} + \frac{(v_{max})^2 - (v_f^{\omega})^2}{2a_L} > x_0^{\omega} \\ \Delta t'^{\omega}_L, & \text{otherwise} \end{cases} \tag{27}$$

where Δt_L^{ω} and $\Delta t'^{\omega}_L$ are calculated in Eqs. (10) and (15). The arrival time at the intersection is

$$t_f^{\omega} = t_0 + \Delta t^{\omega} \tag{28}$$

Case 2: Trajectory Type 2

For a vehicle ω following trajectory Type 2, Newell's linear car-following model (Newell, 2002) is applied. It is described as

$$x^{\omega}(t + \Delta t) = \max \begin{Bmatrix} x^{\omega'}(t + \Delta t - \tau^{\omega}) + d^{\omega}, \\ x^{\omega}(t) - \Delta x_U \end{Bmatrix} \tag{29}$$

where Δt is the time step; Δx_U is the upper bound of the travel distance considering the maximum speed and acceleration rate:

$$\Delta x_U = \begin{cases} v^{\omega}(t)\Delta t + \frac{1}{2}a_U \Delta t^2, & \text{if } \Delta t \le \Delta t' \\ v^{\omega}(t)\Delta t' + \frac{1}{2}a_U \Delta t'^2 + v_{max}\left(\Delta t - \Delta t'\right), & \text{otherwise} \end{cases} \tag{30}$$

where $\Delta t' = (v_{max} - v^{\omega}(t))/a_U$. Therefore, the stationary time headway between a following vehicle and its preceding vehicle is

$$h^{\omega} = \tau^{\omega} + \frac{d^{\omega}}{v_f^{\omega}} \tag{31}$$

The arrival time of following vehicle ω is related to that of its preceding vehicle ω':

$$t_f^{\omega} = t_f^{\omega'} + h^{\omega} \tag{32}$$

3.3. Trajectory generation procedure

Sections 3.1 and 3.2 describe different types of vehicle trajectories for platoon leading vehicles and following vehicles in the same lane given their arrival times at the intersection. However, a platoon leading vehicle may become a following vehicle over time and vice versa. In our trajectory generation procedure, it is not necessary to know whether a vehicle is a leading vehicle or a following vehicle. The trajectories of platoon leading vehicles and following vehicles can be generated in one procedure. The only information needed is the distribution of vehicles across lanes and their arrival times optimized from the MILP model, which will be introduced in the following section.

Given the optimized arrival time t_f^{ω} of vehicle ω in one lane and the current time t_0 (or the optimized travel time $\Delta t^{\omega} = t_f^{\omega} - t_0$), the vehicle trajectory type is identified according to the following steps.

Step 1: If the arrival time remains the same (i.e., $t_f^{\omega} = t'^{\omega}_f$), then vehicle ω maintains its planned trajectory that is optimized in the previous optimization process and go to **Step 4**. Otherwise, go to the next step.

Step 2: If the arrival time of vehicle ω and its preceding vehicle ω' satisfies $t_f^{\omega} = t_f^{\omega'} + h^{\omega}$, then vehicle ω is a following vehicle and follows trajectory Type 2 in Section 3.2 and go to **Step 4**. Otherwise, go to the next step.

Step 3: Vehicle ω may be a platoon leading vehicle in Section 3.1 or a following vehicle that follows trajectory Type 1 in Section 3.2. The trajectories in both cases can be determined according to the solutions to **P1**. Readers can refer to Appendix A for detailed solutions and Feng et al. (2018) for detailed derivation. Go to the next step.

Step 4: The planned trajectory of vehicle ω over the following time is generated.

4. Formulations of optimization model

This section presents the optimization model for vehicle arrival times and traffic signal parameters (i.e., phase sequences, green starts, green durations, and cycle lengths) considering lane-changing behaviors. The objective is vehicle delay minimization. Vehicle trajectory planning is integrated by optimizing vehicle arrival times and lane choices, which determines vehicle delays. The optimization is conducted based on a planning horizon strategy. Basic assumptions, vehicle trajectory constraints, signal constraints, and the objective function are introduced sequentially.

4.1. Assumptions

The following assumptions are made to formulate the optimization problem:

a) Vehicles are homogeneous. The desired speed when passing the intersection is only related to its movement direction.
b) All vehicles are controllable.
c) Vehicles and the signal controller can communicate information in real time within the control zone.
d) Vehicles are in permitted lanes when entering the control zone in each arm. The permitted lanes are the dedicated lanes for a certain vehicle movement.
e) Lane changing behaviors are assumed to be completed instantly.

4.2. Vehicle trajectory constraints

Vehicle trajectory constraints deal with trajectory variables to address the choice of occupied lanes, lane changing behaviors, and vehicle arrival times at the intersection.

4.2.1. Permitted occupied lanes

Each vehicle in arm i occupies only one lane which is specified by

$$\sum_{k\in\mathbf{K}_i}\delta_k^\omega = 1, \forall\omega\in\mathbf{\Omega}_i; i\in\mathbf{I} \tag{33}$$

The occupied lane must be in the set of permitted lanes for vehicle ω:

$$\sum_{k\in\mathbf{K}_\omega}\delta_k^\omega = 1, \forall\omega\in\mathbf{\Omega}_i; i\in\mathbf{I} \tag{34}$$

4.2.2. Possible target lanes

It is assumed that each vehicle ω in each arm i can only select a lane adjacent to the current one as the target lane if vehicle ω is contemplating changing lanes:

$$\sum_{k=\max(k'-1,1)}^{\min(k'+1,|\mathbf{K}_i|)}\delta_k^\omega = 1, \forall\omega\in\mathbf{\Omega}_i; i\in\mathbf{I} \tag{35}$$

where k' is the index of the currently occupied lane of vehicle ω at t_0, and it satisfies:

$$\delta_{k'}^{\prime\omega} = 1 \tag{36}$$

Further, vehicle ω is supposed to maintain its current lane if no preceding vehicles exist:

$$1-\delta_{k'}^\omega \le \sum_{\omega'\in\mathbf{\Omega}_\omega}\boldsymbol{I}_{\{\omega'|\delta'^{\omega'}_{k'}=1,\ x_0^{\omega'}<x_0^\omega\}}(\omega'), \forall\omega\in\mathbf{\Omega}_i; i\in\mathbf{I} \tag{37}$$

where $\boldsymbol{I}_{\mathbf{A}}(x)$ is an indicator function. $\boldsymbol{I}_{\mathbf{A}}(x)=1$, if $x\in\mathbf{A}$; $\boldsymbol{I}_{\mathbf{A}}(x)=0$, otherwise. The right-hand side of Eq. (37) is zero if vehicle ω has no preceding vehicles. This makes $\delta_{k'}^\omega=1$ indicating that vehicle ω keeps its currently occupied lane.

On the other hand, vehicle ω is allowed to move to an adjacent lane k (i.e., $\delta_k^\omega=1$) only if the safety distance between vehicle ω and the vehicles in lane k is guaranteed:

$$\left(x_0^\omega - x_0^{\omega'}\right) - \left(d^\omega + v_0^\omega\tau^\omega + \frac{\left(v_0^\omega\right)^2}{2a_L} - \frac{\left(v_0^{\omega'}\right)^2}{2a_L}\right) \ge -\left(1-\delta_k^\omega\right)\mathrm{M} \tag{38}$$

if $x_0^{\omega'}\le x_0^\omega$

$$\left(x_0^{\omega'} - x_0^\omega\right) - \left(d^{\omega'} + v_0^{\omega'}\tau^{\omega'} + \frac{\left(v_0^{\omega'}\right)^2}{2a_L} - \frac{\left(v_0^\omega\right)^2}{2a_L}\right) \ge -\left(1-\delta_k^\omega\right)\mathrm{M} \tag{39}$$

if $x_0^{\omega'} > x_0^\omega$

$\forall\omega'\in\{\omega'|\delta'^{\omega'}_k=1,\omega'\in\mathbf{\Omega}_i\}; \omega\in\mathbf{\Omega}_i; i\in\mathbf{I}$, where $\max(k'-1,\ 1)\le k\le\min(k'+1,\ |\mathbf{K}_i|)$ and $k\ne k'$. The safety distance in Eqs. (38) and (39) is calculated so that a collision can be avoided when both vehicles decelerate with the maximum deceleration rate.

4.2.3. Lane changing behaviors

The lane changing decision variable μ^ω of vehicle ω is constrained by

$$-\mathrm{M}(1-\mu^\omega) \le \delta'^\omega_k - \delta^\omega_k \le \mathrm{M}(1-\mu^\omega), \forall k \in \mathbf{K}_\omega; \omega \in \mathbf{\Omega}_i; i \in \mathbf{I} \tag{40}$$

$$\mu^\omega \ge \mathrm{M}\left(\delta'^\omega_k + \delta^\omega_k - 2\right) + 1, \forall k \in \mathbf{K}_\omega; \omega \in \mathbf{\Omega}_i; i \in \mathbf{I} \tag{41}$$

When vehicle ω changes lanes, there must be a lane k that satisfies $\delta'^\omega_k \ne \delta^\omega_k$, which means that $\mu^\omega = 0$ by Eq. (40). On the other hand, when vehicle ω maintains its original lane k (i.e., $\exists k \in \mathbf{K}_\omega$ that satisfies $\delta'^\omega_k = \delta^\omega_k = 1$), then $\mu^\omega = 1$ by Eq. (41).

Further, the minimum time interval between two lane changing behaviors is set for safety concerns:

$$t_0 - t^\omega_l - \Delta t^{min}_l \ge -\mathrm{M}\mu^\omega, \forall \omega \in \mathbf{\Omega}_i; i \in \mathbf{I} \tag{42}$$

If $t_0 - t^\omega_l \ge \Delta t^{min}_l$, μ^ω can be either one (i.e., no lane changing) or zero (i.e., lane changing). Otherwise, μ^ω can only be one.

4.2.4. Gap acceptance conditions for lane changing

A vehicle can move into a lane only when the spacing between this vehicle and those vehicles in the target lane is sufficient. That is, after performing lane changing, the spacing between the current vehicle and its preceding and following vehicles in the target lane should both be sufficient, even if the vehicle in the target lane is decelerating (Yeo et al., 2008):

$$x^\omega_0 - x^{\omega'}(t_0 - \tau^\omega) \ge d^\omega - \mathrm{M}\eta^{\omega,\omega'} - \mathrm{M}\mu^\omega, \forall \omega' \in \mathbf{\Omega}_\omega; \omega \in \mathbf{\Omega}_i; i \in \mathbf{I} \tag{43}$$

$$x^\omega_0 - x^{\omega'}(t_0 - \tau^\omega) \ge d^\omega - \mathrm{M}\eta^{\omega,\omega'} - \mathrm{M}\mu^{\omega'}, \forall \omega' \in \mathbf{\Omega}_\omega; \omega \in \mathbf{\Omega}_i; i \in \mathbf{I} \tag{44}$$

$$x^\omega_0 - x^{\omega'}_0 \ge d^\omega + v^\omega_0\tau^\omega + \frac{\left(v^\omega_0\right)^2}{2a_L} - \frac{\left(v^{\omega'}_0\right)^2}{2a_L} - \mathrm{M}\eta^{\omega,\omega'} - \mathrm{M}\mu^\omega \quad \forall \omega' \in \mathbf{\Omega}_\omega; \omega \in \mathbf{\Omega}_i; i \in \mathbf{I} \tag{45}$$

$$x^\omega_0 - x^{\omega'}_0 \ge d^\omega + v^\omega_0\tau^\omega + \frac{\left(v^\omega_0\right)^2}{2a_L} - \frac{\left(v^{\omega'}_0\right)^2}{2a_L} - \mathrm{M}\eta^{\omega,\omega'} - \mathrm{M}\mu^{\omega'} \quad \forall \omega' \in \mathbf{\Omega}_\omega; \omega \in \mathbf{\Omega}_i; i \in \mathbf{I} \tag{46}$$

$x^{\omega'}(t_0 - \tau^\omega)$ is used in Eqs. (43) and (44) for consistence with Eq. (29) in the car-following model. Eqs. (43)–(46) are effective when vehicles ω and ω' are to be in the same lane (i.e., $\eta^{\omega,\omega'} = 0$) after either one changes lanes (i.e., $\mu^\omega = 0$ or $\mu^{\omega'} = 0$). $\eta^{\omega,\omega'}$ is constrained by the following Eqs. (47) and (48):

$$\delta^{\omega'}_k - \eta^{\omega,\omega'} \le \delta^\omega_k \le \delta^{\omega'}_k + \eta^{\omega,\omega'}, \forall k \in \mathbf{K}_\omega \cap \mathbf{K}_{\omega'}; \omega' \in \mathbf{\Omega}_\omega; \omega \in \mathbf{\Omega}_i; i \in \mathbf{I} \tag{47}$$

$$\eta^{\omega,\omega'} \le 2 - \delta^\omega_k - \delta^{\omega'}_k, \forall k \in \mathbf{K}_\omega \cap \mathbf{K}_{\omega'}; \omega' \in \mathbf{\Omega}_\omega; \omega \in \mathbf{\Omega}_i; i \in \mathbf{I} \tag{48}$$

When vehicles ω and ω' are in the same lane ($\eta^{\omega,\omega'} = 0$), Eq. (47) guarantees that $\delta^{\omega'}_k = \delta^\omega_k,\ \forall k \in \mathbf{K}_\omega \cap \mathbf{K}_{\omega'}$. On the other hand, if there is a lane k satisfying $\delta^\omega_k = \delta^{\omega'}_k = 1$, Eq. (48) guarantees that $\eta^{\omega,\omega'} = 0$. Therefore, Eqs. (47) and (48) make $\eta^{\omega,\omega'} = 0$ equivalent to $\delta^{\omega'}_k = \delta^\omega_k,\ \forall k \in \mathbf{K}_\omega \cap \mathbf{K}_{\omega'}$.

4.2.5. Lower and upper bounds of vehicle arrival times

Section 3 builds the relationship between vehicle trajectories and vehicle arrival times at a stop bar for platoon leading vehicles and following vehicles in the same lane. To make the optimal control models feasible, upper and lower bounds of vehicle arrival times are given. Note that a platoon leading vehicle may become a following vehicle over time and vice versa. Instead of setting different travel time bounds for leading and following vehicles respectively, we formulate the bounds that apply to all vehicles.

The lower bound is

$$t^\omega_f \ge t_0 + \Delta t^\omega_L - \mathrm{M}\lambda^\omega, \ \text{if} \ \frac{(v_{max})^2 - \left(v^\omega_0\right)^2}{2a_U} + \frac{(v_{max})^2 - \left(v^\omega_f\right)^2}{2a_L} > x^\omega_0 \quad \forall \omega \in \mathbf{\Omega}_i - \mathbf{\Omega}^p_i; i \in \mathbf{I} \tag{49}$$

$$t^\omega_f \ge t_0 + \Delta t'^\omega_L - \mathrm{M}\lambda^\omega, \ \text{if} \ \frac{(v_{max})^2 - \left(v^\omega_0\right)^2}{2a_U} + \frac{(v_{max})^2 - \left(v^\omega_f\right)^2}{2a_L} \le x^\omega_0 \quad \forall \omega \in \mathbf{\Omega}_i - \mathbf{\Omega}^p_i; i \in \mathbf{I} \tag{50}$$

where Δt^ω_L and $\Delta t'^\omega_L$ are calculated in Eqs. (10) and (15), respectively. Eqs. (49) and (50) indicate that the constraints of minimum arrival time hold for both platoon leading vehicles and following vehicles. The lower bounds are calculated based

on the optimal control models with allowable acceleration rates. Newell's linear car-following model is, however, used to capture the trajectories of following vehicles. To take the inconsistence into consideration, λ^{ω} is used in Eqs. (49) and (50). $\lambda^{\omega}=1$ if vehicle ω keeps its previously optimized trajectory. Then Eqs. (49) and (50) are inactive.

Additionally, vehicle ω cannot overtake its preceding vehicle in the same lane no matter it is a platoon leading vehicle or a following vehicle:

$$t_f^{\omega} \geq t_f^{\omega'} + h^{\omega} - \mathrm{M}\eta^{\omega,\omega'}, \forall \omega' \in \mathbf{\Omega}_{\omega}; \omega \in \mathbf{\Omega}_i - \mathbf{\Omega}_i^p; i \in \mathbf{I} \tag{51}$$

The safety constraint Eq. (51) is borrowed from the car-following model Eq. (32). Eq. (51) is effective only when vehicles ω and ω' are to pass through the intersection in the same lane (i.e., $\eta^{\omega,\omega'}=0$).

The upper bound of arrival time is:

$$t_f^{\omega} \leq t_0 + \Delta t_U^{\omega} + \mathrm{M}\gamma^{\omega}, \forall \omega \in \mathbf{\Omega}_i - \mathbf{\Omega}_i^p; i \in \mathbf{I} \tag{52}$$

where Δt_U^{ω} is calculated in Eq. (11). Similar with λ^{ω} in Eqs. (49) and (50), $\gamma^{\omega}$is used in Eq. (52). $\gamma^{\omega}=0$ if the trajectory of vehicle ω is not affected by all of the preceding vehicles and the trajectory is going to be updated. λ^{ω} and γ^{ω} are constrained as

$$\sum_{\omega' \in \mathbf{\Omega}_{\omega}} \left(1 - \eta^{\omega,\omega'} - \rho^{\omega,\omega'}\right) + \mathrm{M}\lambda^{\omega} \geq \gamma^{\omega}, \forall \omega \in \mathbf{\Omega}_i - \mathbf{\Omega}_i^p; i \in \mathbf{I} \tag{53}$$

$$t_f^{\omega} - t_f^{\omega'} - h^{\omega} \leq \mathrm{M}\eta^{\omega,\omega'} + \mathrm{M}\rho^{\omega,\omega'}, \forall \omega' \in \mathbf{\Omega}_{\omega}, \omega \in \mathbf{\Omega}_i - \mathbf{\Omega}_i^p; i \in \mathbf{I} \tag{54}$$

$$\rho^{\omega,\omega'} \leq 1 - \eta^{\omega,\omega'}, \forall \omega' \in \mathbf{\Omega}_{\omega}, \omega \in \mathbf{\Omega}_i - \mathbf{\Omega}_i^p; i \in \mathbf{I} \tag{55}$$

$$-\mathrm{M}(1-\lambda^{\omega}) \leq t_f^{\omega} - t_f'^{\omega} \leq \mathrm{M}(1-\lambda^{\omega}), \forall \omega \in \mathbf{\Omega}_i - \mathbf{\Omega}_i^p; i \in \mathbf{I} \tag{56}$$

where $\rho^{\omega,\omega'}$ is an introduced binary variable. Eqs. (54) and (55) ensure that $\rho^{\omega,\omega'}=1$ when the trajectory of vehicle ω is not affected by its preceding vehicle ω' (i.e., $\eta^{\omega,\omega'}=0$ and $t_f^{\omega} > t_f^{\omega'} + h^{\omega}$). Eqs. (53) and (56) indicate that the upper bound constraint (52) is only effective ($\gamma^{\omega}=0$) if vehicle ω is not affected by all the preceding vehicles ($\sum_{\omega' \in \mathbf{\Omega}_{\omega}}(1 - \eta^{\omega,\omega'} - \rho^{\omega,\omega'}) = 0$) and its trajectory is going to be updated ($\lambda^{\omega}=0$).

4.2.6. No-changing zones

Vehicles in no-changing zones keep their previously optimized trajectories. That is, the trajectories of these vehicles will not be updated with varying traffic condition. The benefits of doing so are to reduce computational burden but at the cost of optimality. The constraints are specified by

$$\delta_k^{\omega} = \delta'^{\omega}_k, \forall k \in \mathbf{K}_i; \omega \in \mathbf{\Omega}_i^p; i \in \mathbf{I} \tag{57}$$

$$t_f^{\omega} = t_f'^{\omega}, \forall \omega \in \mathbf{\Omega}_i^p; i \in \mathbf{I} \tag{58}$$

Eqs. (57) and (58) guarantee no lateral (i.e., lane-changing behaviors) and longitudinal trajectory (i.e., arrival time at stop bars) changes, respectively. According to the trajectory generation procedure in Section 3.3, maintaining the previously optimized arrival time is equal to maintaining the previously planned trajectories.

4.3. Signal constraints

Signal constraints deal with signal parameters in an optimization horizon. Vehicle trajectory planning is integrated into signal optimization with the aid of vehicle arrival times and lane choices. Phase sequences, green start and duration of each phase, and cycle lengths are optimized.

4.3.1. Lane signal settings

If the traffic flow from arm i to arm j is permitted in several lanes ($\zeta_k^{i,j}=1$), then vehicles in these lanes must receive identical signal indication:

$$\begin{aligned} &-\mathrm{M}\left(1-\zeta_k^{i,j}\right) \leq \Theta_{i,k}^n - \theta_{i,j}^n \leq \mathrm{M}\left(1-\zeta_k^{i,j}\right) \\ &\forall n = 1,\ldots,N; k \in \mathbf{K}_i; (i,j) \in \mathbf{\Psi}; i \in \mathbf{I} \end{aligned} \tag{59}$$

$$\begin{aligned} &-\mathrm{M}\left(1-\zeta_k^{i,j}\right) \leq \Phi_{i,k}^n - \phi_{i,j}^n \leq \mathrm{M}\left(1-\zeta_k^{i,j}\right) \\ &\forall n = 1,\ldots,N; k \in \mathbf{K_i}; (i,j) \in \mathbf{\Psi}; i \in \mathbf{I} \end{aligned} \tag{60}$$

where $\theta_{i,j}^n$ and $\phi_{i,j}^n$ are the green start and green duration for traffic flow (i, j) in the n^{th} cycle; $\Theta_{i,k}^n$ and $\Phi_{i,k}^n$ are the green start and green duration in lane k of arm i in the n^{th} cycle. These constraints ensure that $\Theta_{i,k}^n = \theta_{i,j}^n$ and $\Phi_{i,k}^n = \phi_{i,j}^n$, i.e., identical signal settings for all permitted lanes k.

4.3.2. Green start time

Since phase sequences are not determined in advance, the green start time of each phase in every cycle is confined in one cycle length:

$$t_s + \sum_{n'=1}^{n-1} C^{n'} \le \theta_{i,j}^n \le t_s + \sum_{n'=1}^{n} C^{n'}, \forall (i,j) \in \mathbf{\Psi}; n = 1, \ldots, N \tag{61}$$

However, the green start time is known if the phase was already started or terminated before time t_0 in the first cycle as shown in Eqs. (62) and (63), respectively:

$$\theta_{i,j}^n = \theta_{i,j}^0, \forall n = 1; (i,j) \in \mathbf{\Psi}_0 \tag{62}$$

$$\theta_{i,j}^n = \theta_{i,j}^p, \forall n = 1; (i,j) \in \mathbf{\Psi}_p \tag{63}$$

The green start times for the phases that will receive green after time t_0 in the first cycle are constrained in Eq. (64):

$$\theta_{i,j}^n \ge t_0, \forall n = 1; (i,j) \in \mathbf{\Psi} - \mathbf{\Psi}_0 - \mathbf{\Psi}_p \tag{64}$$

4.3.3. Duration of green

For safety concerns, a minimum value of green duration is set in Eq. (65):

$$g_{min}^{i,j} \le \phi_{i,j}^n \le C^n, \forall (i,j) \in \mathbf{\Psi}; n = 1, \ldots, N \tag{65}$$

The green durations for the phases whose greens were terminated before time t_0 in the first cycle are fixed:

$$\phi_{i,j}^n = \phi_{i,j}^p, \forall n = 1; (i,j) \in \mathbf{\Psi}_p \tag{66}$$

The green durations for the phases that are green at time t_0 in the first cycle are constrained:

$$\phi_{i,j}^n \ge t_0 - \theta_{i,j}^n, \forall n = 1; (i,j) \in \mathbf{\Psi}_0 \tag{67}$$

4.3.4. Green end time

The proposed control strategies are able to generate compact vehicle platoons. At most one platoon can pass through the intersection in one lane during one cycle. The green start and end times for each phase should be in the same cycle:

$$t_s + \sum_{n'=1}^{n-1} C^{n'} \le \theta_{i,j}^n + \phi_{i,j}^n \le t_s + \sum_{n'=1}^{n} C^{n'}, \forall (i,j) \in \mathbf{\Psi}; n = 1, \ldots, N \tag{68}$$

4.3.5. Cycle length

Consider the start time t_s of the optimization horizon and the current time t_0, the cycle length of the first cycle is constrained in Eq. (69):

$$C^n \ge t_0 - t_s, n = 1 \tag{69}$$

4.3.6. Phase sequence

Traffic flows (i, j) and (l, m) are incompatible if they cannot have right of way at the same time. The phase sequence that avoids incompatible traffic flows in each cycle are constrained as:

$$\Lambda_{i,j,l,m}^n + \Lambda_{l,m,i,j}^n = 1, \forall ((i,j),(l,m)) \in \mathbf{\Psi}_{ic}; n = 1, \ldots, N \tag{70}$$

4.3.7. Clearance time

For a pair of incompatible traffic flows, the following constraints are specified to ensure the clearance time:

$$\theta_{i,j}^n + \phi_{i,j}^n + \pi_{i,j,l,m} \le \theta_{l,m}^n + \mathrm{M}\left(1 - \Lambda_{i,j,l,m}^n\right) \quad \forall ((i,j),(l,m)) \in \mathbf{\Psi}_{ic}; n = 1, \ldots, N \tag{71}$$

$$\theta_{l,m}^n + \phi_{l,m}^n + \pi_{l,m,i,j} \le \theta_{i,j}^n + \mathrm{M}\left(1 - \Lambda_{l,m,i,j}^n\right) \quad \forall ((i,j),(l,m)) \in \mathbf{\Psi}_{ic}; n = 1, \ldots, N \tag{72}$$

If traffic flow (l, m) follows (i, j) in the n^{th} cycle, i.e., $\Lambda_{i,j,l,m}^n = 1$, constraint Eq. (71) is effective. Otherwise, constraint Eq. (72) is effective.

Moreover, the clearance time between the traffic flows in subsequent cycles should also be guaranteed:

$$\theta_{i,j}^n + \phi_{i,j}^n + \pi_{i,j,l,m} \le \theta_{l,m}^{n+1}, \forall (i,j) \in \mathbf{\Psi}; (l,m) \in \mathbf{\Psi}; n = 1, \ldots, N-1 \tag{73}$$

Similarly, the clearance time between the first traffic flow in the first cycle and the last traffic flow in the N^{th} cycle should also be guaranteed:

$$\theta_{i,j}^N + \phi_{i,j}^N + \pi_{i,j,l,m} \le \theta_{l,m}^1 + \sum_{n=1}^{N} C^n, \forall (i,j) \in \mathbf{\Psi}; (l,m) \in \mathbf{\Psi} \tag{74}$$

4.3.8. Vehicle arrival times at stop bars

Due to vehicle trajectory planning, vehicles in the same lane are turned into compacted platoons to pass through the intersection within green intervals $[\Theta_{i,k}^n, \Theta_{i,k}^n + \Phi_{i,k}^n]$. Queues at stop bars are avoided for full utilization of intersection capacity. A binary variable β_n^ω is defined to distribute vehicles to different cycles. Let $\beta_n^\omega = 1$ if vehicle ω is supposed to pass through the intersection in the n^{th} cycle; and $\beta_n^\omega = 0$, if in other cycles. The constraints of arrival time t_f^ω are expressed as

$$\begin{aligned} &\Theta_{i,k}^n - \mathrm{M}\left(1 - \delta_k^\omega\right) - \mathrm{M}(1 - \beta_n^\omega) \le t_f^\omega \\ &\le \Theta_{i,k}^n + \Phi_{i,k}^n + \mathrm{M}\left(1 - \delta_k^\omega\right) + \mathrm{M}(1 - \beta_n^\omega) \\ &\forall n = 1, \ldots, N; k \in \mathbf{K}_\omega; \omega \in \mathbf{\Omega}_i; i \in \mathbf{I} \end{aligned} \tag{75}$$

Eq. (75) is effective when vehicle ω is supposed to pass the stop bar in lane k ($\delta_k^\omega = 1$) in the n^{th} cycle ($\beta_n^\omega = 1$). Further, vehicle ω can choose only one of the N cycles in the signal optimization horizon:

$$\sum_{n=1}^{N} \beta_n^\omega = 1, \forall \omega \in \mathbf{\Omega}_i; i \in \mathbf{I} \tag{76}$$

4.3.9. Other signal constraints

In practice, there may be some constraints on the relative timing of green starts and ends for different traffic flows. Define $z_{i,j,l,m}^{n,s}$ and $z_{i,j,l,m}^{n,e}$ as the relative time for green starts and ends measured from traffic flow (i, j) to (l, m) in each cycle, respectively. The constraints are specified as

$$\theta_{i,j}^n + z_{i,j,l,m}^{n,s} = \theta_{l,m}^n, \forall (i,j) \in \mathbf{\Psi}; (l,m) \in \mathbf{\Psi}; n = 1, \ldots, N \tag{77}$$

$$\theta_{i,j}^n + \phi_{i,j}^n + z_{i,j,l,m}^{n,\,e} = \theta_{l,m}^n + \phi_{l,m}^n, \forall (i,j) \in \mathbf{\Psi}; (l,m) \in \mathbf{\Psi}; n = 1, \ldots, N \tag{78}$$

These constraints are mainly used to make sure that two signal groups start or end simultaneously (i.e., $z_{i,j,l,m}^{n,s} = 0$ or $z_{i,j,l,m}^{n,e} = 0$) for practical considerations.

4.4. Optimization models

The primary objective of the proposed optimization model is the minimization of vehicle travel delays. The travel delay of each vehicle is defined as the difference between the actual travel time and the free flow travel time. It is noticed that there may be multiple solutions that have the same total vehicle delay but with different cycle lengths. Since we have no constraints of maximum cycle lengths or maximum phase green times to make the model more flexible, a secondary objective of cycle length minimization is added. It increases the frequency of switching right of way and potentially decreases the delays of the incoming vehicles in the future. The proposed model is a hierarchical multi-objective optimization model. Total vehicle delay is first minimized and then cycle lengths are minimized for the solutions with the same minimum delay. The most common approach to such a model is the weighted sum method (Marler and Arora, 2004). As a result, the objective function is formulated as

P3:

$$\min_{\boldsymbol{V}=(\tilde{\boldsymbol{T}},\boldsymbol{S})} \alpha_1 \sum_{i \in \mathbf{I}} \sum_{\omega \in \mathbf{\Omega}_i} \left(t_f^\omega - t_e^\omega - \frac{L_i}{v_{max}} \right) + \alpha_2 \sum_{n=1}^{N} C^n \tag{79}$$

where $\tilde{\boldsymbol{T}}$ is a subset of the trajectory variable set $\boldsymbol{T}$ in Table 2 (i.e., $\tilde{\boldsymbol{T}} = \boldsymbol{T} - \{x^\omega(t),\ l^\omega(t), v^\omega(t), a^\omega(t)\}$); α_1 and α_2 are weighting parameters and $\alpha_1 \gg \alpha_2 > 0$. The constraints are Eqs. (33)–(78). $t_f^\omega - t_e^\omega$ is the actual travel time of vehicle ω. Note that $t_f^\omega - t_e^\omega$ also includes the waiting time before entering the control zone when there is a queue at the boundary of a control zone. L_i/v_{max} is the free flow travel time. The objection function and all constraints are linear. Therefore, the optimization model (**P3**) is an MILP problem that can be solved by many existing algorithms or commercial solvers.

In the MILP model, the number of effective binary variables is $\sum_{i \in \mathbf{I}} \sum_{\omega \in \mathbf{\Omega}_i - \mathbf{\Omega}_i^p} (|\mathbf{K}_i| + |\mathbf{\Omega}_\omega| + N + 3)$. The number of effective continuous variables is $\sum_{i \in \mathbf{I}} (|\mathbf{\Omega}_i - \mathbf{\Omega}_i^p| + 2N|\mathbf{K}_i|) + N(2|\mathbf{\Psi}| + |\mathbf{\Psi}_{ic}| + 1)$. The number of effective trajectory constraints is bounded by $\sum_{i \in \mathbf{I}} \sum_{\omega \in \mathbf{\Omega}_i - \mathbf{\Omega}_i^p} (10 + |\mathbf{\Omega}_i| + 2|\mathbf{K}_\omega| + (7 + |\mathbf{K}_i|)|\mathbf{\Omega}_\omega|)$. And the number of effective signal constraints is $\sum_{i \in \mathbf{I}} (2N|\mathbf{\Psi}||\mathbf{K}_i|) + \sum_{i \in \mathbf{I}} \sum_{\omega \in \mathbf{\Omega}_i} (1 + N|\mathbf{K}_\omega|) + (3N + 1)|\mathbf{\Psi}| + |\mathbf{\Psi}_0| + |\mathbf{\Psi}_p| + (3N - 1)|\mathbf{\Psi}_{ic}| + 3N|\mathbf{\Psi}|^2$. The complexity of the MILP model mainly depends on the vehicle number in the control zone. The numbers of binary and continuous variables exhibit quadratic and linear growth with respect to the vehicle number $|\mathbf{\Omega}_i|$ in each arm in the worst cases, respectively. The constraint number shows quadratic growth with respect to $|\mathbf{\Omega}_i|$ in the worst cases as well.

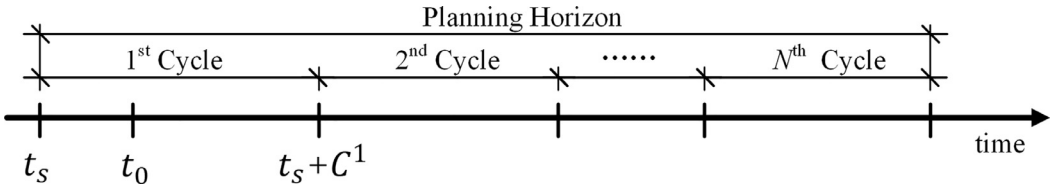

Fig. 5. Illustration of planning horizon.

4.5. Impacts of weighting parameters on solution quality

Generally, **P3** is not equivalent to the original hierarchical multi-objective optimization model. Intuitively, cycle length minimization in **P3** urges vehicles to pass through the intersection within less time and thus leads to less delay. However, in theory, **P3** may produce a solution with worse quality in terms of total vehicle delay. Denote d_1 and C_1^n as the minimum total vehicle delay and the length of the n^{th} cycle given by the original hierarchical multi-objective optimization model. Denote d_2 and C_2^n as the total vehicle delay and the cycle length of any solution given by **P3**. We have

$$\alpha_1 d_1 + \alpha_2 \sum_{n=1}^{N} C_1^n = \alpha_1 d_2 + \alpha_2 \sum_{n=1}^{N} C_2^n \tag{80}$$

where $d_2 \geq d_1$ and $\sum_{n=1}^{N} C_2^n \leq \sum_{n=1}^{N} C_1^n$. Then we get

$$\alpha_1 (d_2 - d_1) = \alpha_2 \left(\sum_{n=1}^{N} C_1^n - \sum_{n=1}^{N} C_2^n \right) \tag{81}$$

If $d_2 = d_1$ and $\sum_{n=1}^{N} C_1^n = \sum_{n=1}^{N} C_2^n$, then the solution to **P3** is also the solutions to the original model. Otherwise, we have

$$d_2 - d_1 = \frac{\alpha_2}{\alpha_1} \left(\sum_{n=1}^{N} C_1^n - \sum_{n=1}^{N} C_2^n \right) \leq \Delta d \tag{82}$$

where Δd is the tolerance of solution quality degradation. To guarantee Eq. (82), α_1/α_2 is expected to satisfy the following Eq. (83) in a conservative way:

$$\frac{\alpha_1}{\alpha_2} \geq \frac{\sum_{n=1}^{N} C_1^n}{\Delta d} \tag{83}$$

Although $\sum_{n=1}^{N} C_1^n$ is unknown, its upper bound can be easily estimated by solving a special case of **P3** with $\alpha_1 = 1$ and $\alpha_2 = 0$, i.e., only minimizing total vehicle delay. The resultant signals are divided into two parts by the passing time of the last vehicle. The 2nd part, i.e., the signals after the passing time of the last vehicle, may be unrealistic because of too large cycle lengths. But it has no impacts on vehicle delays. The length of this part can then be recalculated based on minimum green durations. The upper bound is the total length of the 1st part and the 2nd part and is used to replace $\sum_{n=1}^{N} C_1^n$ in Eq. (83) as the guide to the selection of α_1 and α_2 in each optimization.

4.6. Planning horizon procedure

Previous studies use time (in seconds) as the length of the planning horizon with a fixed number of cycles (Feng et al., 2015), which is different in this study. The cycle number N in the planning horizon, as shown in Fig. 5, depends on the number of vehicles considered in the optimization. Note that cycle lengths are optimized over time and, therefore, the total time of the planning horizon may vary over time as well. Based on the constraints in Section 4.3.8, N needs to be large enough so that all vehicles are planned to pass through the intersection in the N cycles. A smaller N may render the optimization model infeasible while a larger N increases computational burden. As a result, we choose the smallest N that makes the model feasible. Note that the choice of N has no impacts on solution optimality under the condition that the MILP model is feasible. The planning horizon procedure is shown in Fig. 6, which follows:

Step 1: Initialize horizon start time $t_s = 0$ and cycle number $N = 1$ at initial time $t_0 = 0$.
Step 2: Collect information of vehicles in the control zone at time t_0.
Step 3: Solve the special case of the MILP model **P3** with $\alpha_1 = 1$ and $\alpha_2 = 0$.
Step 4: If the model is infeasible, then update the cycle number $N = N + 1$ and go to **Step 3**. Otherwise, go to the next step.
Step 5: Select α_1 and α_2 as explained in Section 4.5 so that α_1/α_2 is large enough.
Step 6: Solve the MILP model **P3**.

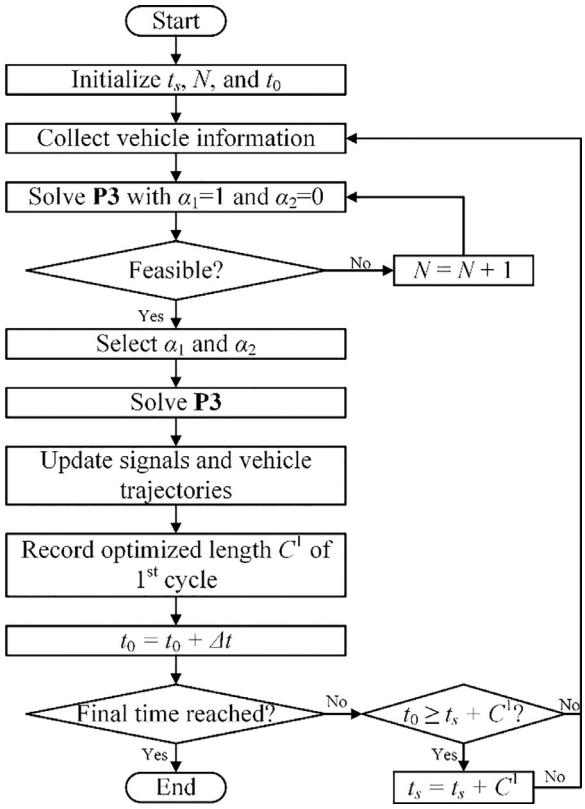

Fig. 6. Planning horizon procedure.

Table 3
Basic traffic demand and volume/capacity ratios.

Traffic demand in pcu/h (v/c)	To Arm			
From Arm	1	2	3	4
1	–	200 (0.38)	400 (0.35)	100 (0.21)
2	150 (0.32)	–	150 (0.29)	200 (0.35)
3	380 (0.33)	150 (0.32)	–	180 (0.35)
4	100 (0.19)	200 (0.35)	100 (0.21)	–

Step 7: Update the signals and the planned vehicle trajectories in the control zone according to the optimization results.
Step 8: Record the optimized length C^1 of the first cycle.
Step 9: Update time $t_0 = t_0 + \Delta t$, where Δt is the time step.
Step 10: If t_0 reaches the final simulation time, then end the process. Otherwise, go to the next step.
Step 11: If $t_0 \geq t_s + C^1$, then update $t_s = t_s + C^1$. Go to **Step 2**.

5. Numerical examples

5.1. Experimental data

To evaluate the proposed models, a typical four-arm intersection with all directions of movements is applied. The lane markings of the intersection are shown in Fig. 7. Right-turning vehicles are not controlled by traffic signals but they are controlled to arrive at the intersection at a desired speed. The length L_i of the control zone in each arm is 300 m which is the reliable communication range of Dedicated Short-Range Communications (DSRC) (Emmelmann et al., 2010). The length L_i^p of the no-changing zone in each arm is 50 m.

The basic traffic demand and the volume/capacity (v/c) ratios are shown in Table 3. The v/c ratios are calculated with the assumed green duration of 26 s for each phase and a cycle length of 120 s. The saturation flow in each lane is determined by the time headway in Eq. (31). Vehicles are generated according to Poisson distribution, which is a common practice for traffic control at isolated intersections (Jiang et al., 2017; Li et al., 2014). Speed limit v_{max} is 15 m/s. The desired speeds v_f^ω of

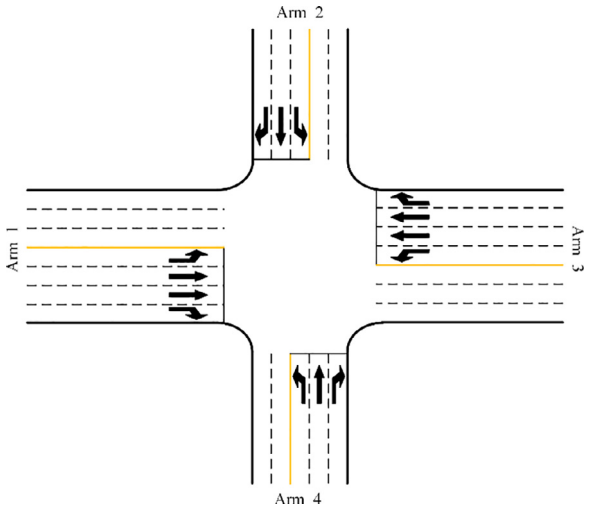

Fig. 7. Lane markings of a four-arm intersection.

Table 4
Throughput.

Demand factor	Throughput (veh)		
	Actuated Control	CAV-based Control	Increase (%)
0.6	289.60	291.20	0.55
1.0	446.00	449.20	0.72
2.0	686.00	691.50	0.80
3.0	764.60	824.80	7.87
4.0	769.70	922.10	19.80

left-turning, though, and right-turning vehicles passing through the intersection are 10 m/s, 13 m/s, and 8 m/s, respectively. Vehicles enter the control zone at the speed of 13 m/s instead of the speed limit in order to test more cases in the trajectory generation in Appendix A. The time displacement τ^{ω} and space displacement d^{ω} in the car-following model are 0.9 s (assuming quick reaction of CAVs) and 6 m. The minimum time interval between two lane changing behaviors of a vehicle is 5 s. The absolute values of the maximum comfortable acceleration and deceleration rates (a_U and a_L) are 2 m/s^2 and 4 m/s^2. The clearance time $\pi_{i,j,\,l,\,m}$ between incompatible traffic flows (e.g., the traffic flow from arm 1 to arm 2 and the traffic flow from arm 2 to arm 3) is 4 s. The minimum green time $g_{min}^{j,j}$ is 6 s. The tolerance Δd of solution quality degradation is 3 s. The weighting parameters α_1 and α_2 in the objective function Eq. (79) are 300 and 1, which satisfy Eq. (83) in each optimization. To investigate the environmental impacts, the CO_2 emission model in Frey et al., (2002) is employed.

The optimization models are written in C# and solved using Gurobi 7.5.1 (Gurobi Optimization Inc., 2017). All the experiments are performed in a desktop computer with an Intel 3.6 GHz CPU and 16 GB memory. An upper limit of 1.5 s is set for real-time application. A sub-optimal solution produced by the solver will be accepted if the solving time exceeds the time limit.

5.2. Results and discussions

Vehicle-actuated control is applied in the simulation as the benchmark for comparison with the proposed control method, denoted as CAV-based control. In actuated control, the maximum green durations for arm 1 and arm 3 are 30 s, and the maximum green duration for arm 2 and arm 4 are 20 s. The minimum green duration is 4 s which is the optimal value by trial and error. The unit extension time is 2 s. The time of each simulation scenario is 1200 s and the simulation time step is 1 s. Average values of throughput, vehicle delays, and CO_2 emissions of ten different random seeds are recorded and shown in Tables 4–6. Five levels of traffic demand are tested, which are the product of the basic demand and a demand factor. The demand with the factors from 0.6 to 2.0 is under-saturated and the demand with factors 3.0 and 4.0 are over-saturated. The under-saturated and over-saturated traffic condition is observed with actuated control.

Table 4 shows that CAV-based control improves intersection capacity. The throughput increase under CAV-based control is insignificant with under-saturated traffic demand. This is consistent with our intuition because demand is below intersection capacity under both control methods. When the demand factor further increases to 3.0 and 4.0, intersection capacity is reached under actuated control because the throughput almost remains the same. In contrast, the throughput

Table 5
Average delay.

Demand factor	Average Delay (s/veh)		
	Actuated Control	CAV-based Control	Decrease (%)
0.6	14.65	8.62	41.16
1.0	15.84	11.33	28.47
2.0	18.32	13.59	25.82
3.0	61.71	15.40	75.04
4.0	98.28	16.34	83.37

Table 6
Average CO_2 emissions.

Demand factor	Average CO_2 Emissions (g/veh)		
	Actuated Control	CAV-based Control	Decrease (%)
0.6	123.96	114.73	7.45
1.0	126.19	123.51	2.12
2.0	134.98	132.38	1.93
3.0	212.65	133.08	37.42
4.0	267.07	135.39	49.31

under CAV-based control keeps increasing noticeably. This indicates that intersection capacity under CAV-based control is higher compared with actuated control.

Table 5 shows the significant decrease of vehicle delays when CAV-based control is applied, which can reach ~40% under low traffic demand and ~80% under high demand. The benefits are mainly due to improved intersection capacity as well as the more efficient use of green time at the intersection. Vehicle trajectories are optimized so that all vehicles pass through the intersection at high desired speeds without stops. Thus, no vehicle queues are generated at stop bars, either. As a result, the green start-up lost time is eliminated and more vehicles can pass the intersection during the same green interval compared with actuated control. One interesting observation is that the delay reduction under CAV-based control decreases first and then rises as demand increases. Under under-saturated demand, the benefits are more remarkable with lower demand which indicates strong flow uncertainty. Under over-saturated demand, the delay under actuated control rises more significantly as demand increases. Because the intersection capacity under CAV-based control is much higher than that under actuated control.

Table 6 shows the comparison of CO_2 emissions. The results are similar to those in Table 5. CAV-based control outperforms actuated control under both under- and over-saturated demand. This is intuitive because the trajectories of platoon leading vehicles are planned with the aim of reducing fuel consumption/emission. Following vehicles also have smoother trajectories since they do not make complete stops at stop bars. But the benefits decrease with increasing traffic volumes with under-saturated demand. The reason is that vehicles are likely to accelerate or decelerate more frequently under CAV-based control when traffic condition varies. As shown in Fig. 8, vehicles decelerate only once before arriving at the intersection under actuated control while vehicles keep adjusting their speeds according to varying traffic condition under CAV-based control. However, the benefits are significant under over-saturated demand. Because intersection capacity is improved under CAV-based control and thus vehicles experience much less delays. This indicates that vehicles spend much less time traversing the intersection. In this way, CO_2 emissions are greatly reduced.

5.3. Sensitivity analysis

5.3.1. Minimum green time

Minimum green time is designed to guarantee safety. It may be reduced when every vehicle is controllable and the pedestrian flow can be ignored (e.g., intersections with overpasses for pedestrians). In that case, the proposed model is likely to bring more benefits. To this end, a sensitivity analysis of minimum green time is performed to explore the potential benefits. The experiments show that a smaller minimum green duration results in significantly smaller vehicle delays and lower CO_2 emissions under CAV-based control, as shown in Fig. 9. When the minimum green time decreases from 6 s to 1 s, the CO_2 emissions and average vehicle delay under CAV-based control both decrease notably compared with actuated control. For example, the decreases of CO_2 emissions and vehicle delays reach ~16% and ~70%, respectively, when the minimum green duration is 1 s. This is reasonable because a smaller minimum green duration helps avoid green waste time due to flow fluctuations, especially under low demand. A small green duration can be used for efficiency, similar with the consideration of skipping a phase in some signalization approaches. In current practice, the minimum green duration is usually set to at least 5 seconds. However, it can be reduced to a smaller value under CAV-based control since no driver reaction time and human errors need to be considered.

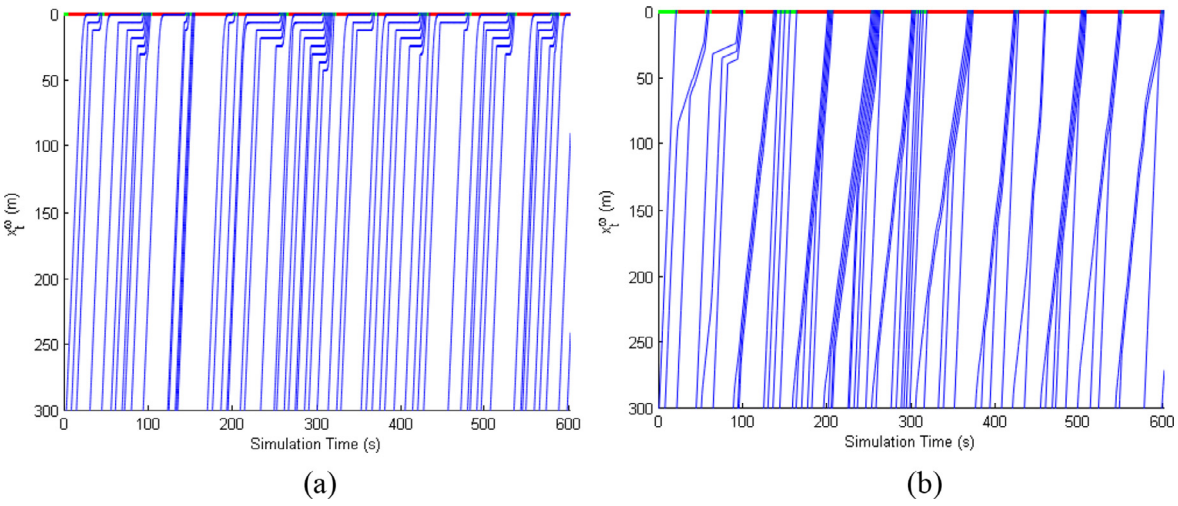

Fig. 8. Trajectories of left-turning vehicles in arm 1 as an example: (a) actuated control, and (b) CAV-based control.

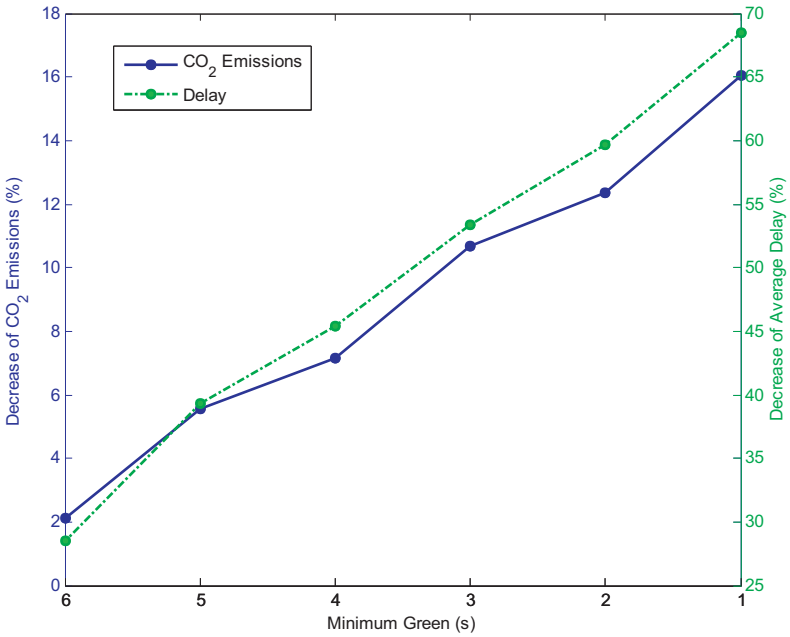

Fig. 9. Decrease of CO_2 emissions and vehicle delays with decreasing minimum green under CAV-based control compared with actuated control. (For interpretation of the references to colour in this figure legend, the reader is referred to the web version of this article.)

5.3.2. Length of no-changing zones

The purpose of setting no-changing zones is to reduce computational burden at the cost of optimality. Vehicles within no-changing zones keep their previously planned trajectories. Thus, the number of vehicles considered in the proposed MILP model is reduced. Fig. 10 shows the impacts of the length of no-changing zones on the performance of CAV-based control. Four demand levels from low to high are tested with the demand factors from 1.0 to 4.0. Fig. 10(a) shows that the length of no-changing zones has no significant impacts on the throughput at all demand levels. This is because the demand has not reached the intersection capacity, as discussed in Section 5.2. Fig. 10(b) shows that vehicle delays increase with increasing length of no-changing zones. The delay increase is more significant with a longer length of no-changing zones under high demand (demand factors 3 and 4). Fig. 10(c) shows similar results to Fig. 10(b) but in terms of CO_2 emissions. Therefore, the setting of no-changing zones does not have much negative impact on the performance of the model if traffic demand is not high and the zone length is not too long.

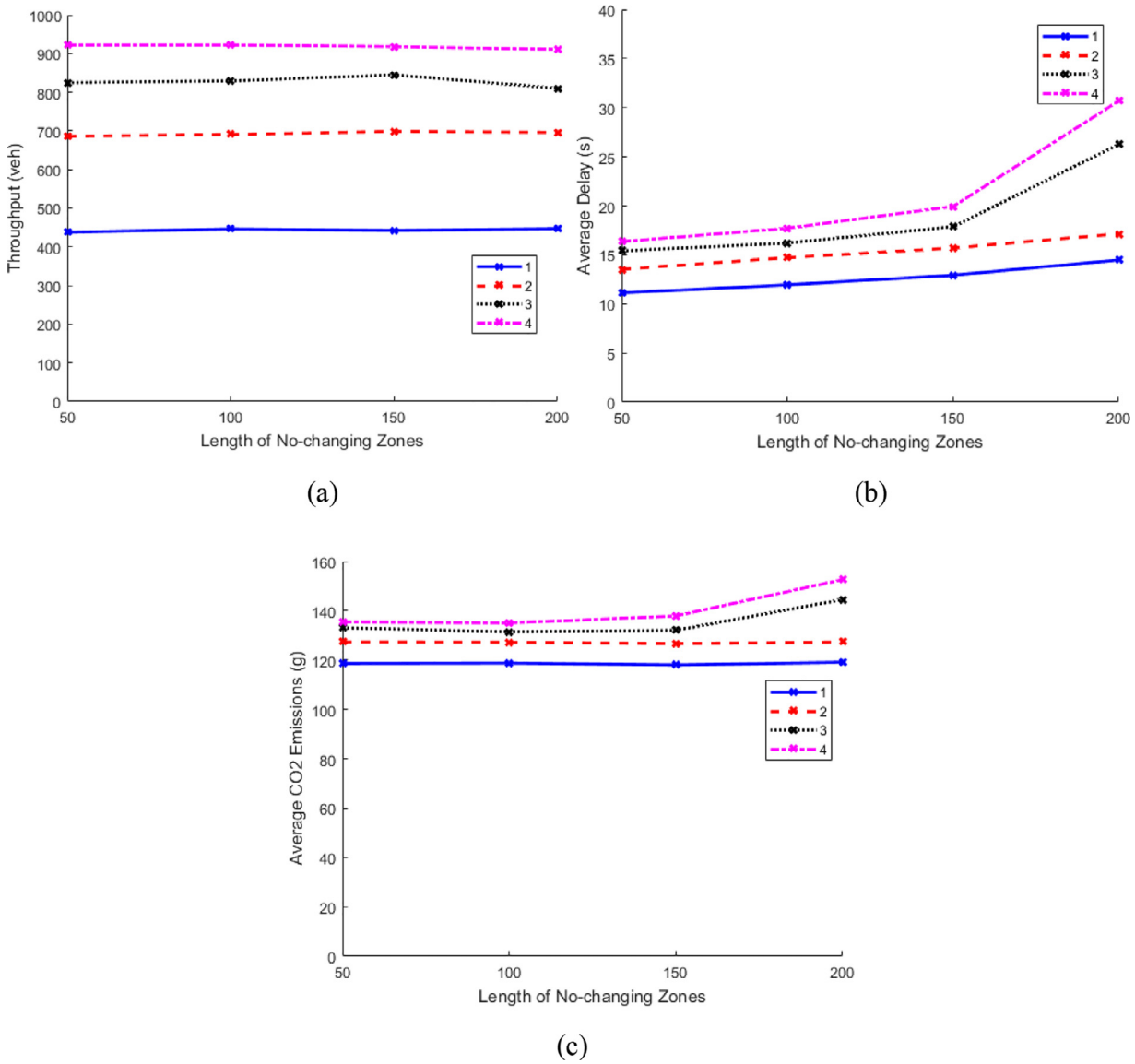

Fig. 10. Impacts of the length of no-changing zones: (a) throughput, (b) vehicle delays, and (c) CO_2 emissions.

6. Conclusions and recommendations

This research develops an MILP model that optimizes vehicle trajectories and traffic signals in a unified framework at isolated urban intersections with multiple phases and all directions of vehicle movements. Phase sequences, green start and duration of each phase, and cycle lengths are optimized together with vehicle lane-changing behaviors and arrival times for vehicle delay minimization. Vehicle trajectory planning is integrated into signal optimization via the lane choice and the arrival time of each vehicle at stop bars. A planning horizon strategy is applied to conduct the optimization. Vehicles are grouped into platoons and are guaranteed to pass through the intersection at desired speeds to avoid stops at stop bars. The trajectories of vehicles in each lane are planned based on optimized vehicle arrival times. Simulation results show that the proposed CAV-based control outperforms vehicle-actuated control in terms of intersection capacity, vehicle delay, and CO_2 emissions. A sensitivity analysis is conducted to show the potential benefits of a small minimum green duration as well as the impacts of no-changing zones on the optimality of the proposed control.

It is assumed that all vehicles are controllable which may restrict the implementation of the proposed model. To relax this assumption for lower market penetration of CAVs, more constraints including the choice of platoon leading vehicles and the consideration of queues at stop bars are necessary. A car-following model is used to capture following vehicle trajectories, which provides the potential for extending the current work to mixed traffic condition. The proposed model lays

the foundation for implementing more complicated and realistic traffic conditions, where the un-controllable vehicles can be described by the car-following model. For simplicity, homogeneous vehicles are assumed and vehicles in the same lane have same desired speed upon arriving at the intersection. It is interesting to extend the model to heterogeneous vehicles, for example, in the case with shared lanes. For real-world implementation, the uncertainties in vehicle driving behaviors and traffic environment cannot be ignored. Furthermore, we plan to expand this model to optimize vehicle trajectories and signal timings at a network level. The combination of the proposed model and the reservation-based models is also worth investigating.

Acknowledgments

This research was partially funded by the US Department of Energy (EERE Award No. DE-EE0007212) and China Scholarship Council (No. 201506260033). The views presented in this paper are those of the authors alone.

Appendix A. Trajectory generation for leading vehicles

Given the optimized arrival time t_f^ω of vehicle ω and the current time t_0 (or the optimized travel time $\Delta t^\omega = t_f^\omega - t_0$), the optimal trajectory of ω is identified by solving **P1**. The solutions are among six scenarios. Please refer to Feng et al. (2018) for detailed derivation.

Scenario 1: $\Delta t^\omega = \Delta t_L^\omega$

As shown in constraint Eq. (12), the minimum travel time of vehicle ω is Δt_L^ω that is calculated in Eq. (10). This scenario only happens in Case 1 in Section 3.1. When $\Delta t^\omega = \Delta t_L^\omega$, vehicle ω has to accelerate with a_U to speed $v^\omega(t_1^\omega)$ at location $x^\omega(t_1^\omega)$ at time t_1^ω and then it decelerates with $-a_L$ until reaching the intersection with speed v_f^ω at time t_f^ω. t_1^ω, $x^\omega(t_1^\omega)$, and $v^\omega(t_1^\omega)$ are calculated as

$$t_1^\omega = t_0 + \frac{v_f^\omega - v_0^\omega + a_L \Delta t^\omega}{a_U + a_L} \tag{84}$$

$$v^\omega(t_1^\omega) = v_0^\omega + a_U(t_1^\omega - t_0) \tag{85}$$

$$x^\omega(t_1^\omega) = x_0^\omega - \frac{v_0^\omega + v^\omega\left(t_1^\omega\right)}{2}(t_1^\omega - t_0) \tag{86}$$

The notations are explained in Tables 1 and 2. Note that only the deceleration segment exists if $v_0^\omega = v_f^\omega + a_L(t_f^\omega - t_0)$.

Scenario 2: $\Delta t_L^\omega < \Delta t^\omega < \Delta t_{OL}^\omega$

The travel time Δt_{OL}^ω is calculated as

$$\Delta t_{OL}^\omega = \begin{cases} \dfrac{x_0^\omega}{v_0^\omega} + \dfrac{\left(v_0^\omega - v_f^\omega\right)^2}{2 v_0^\omega a_L}, & \text{if } v_0^\omega \geq v_f^\omega \\ \dfrac{x_0^\omega}{v_f^\omega} + \dfrac{\left(v_0^\omega - v_f^\omega\right)^2}{2 v_f^\omega a_U}, & \text{otherwise} \end{cases} \tag{87}$$

In this scenario, vehicle ω accelerates with a_U to speed $v^\omega(t_1^\omega)$ at location $x^\omega(t_1^\omega)$ at time t_1^ω, maintains this speed until time t_2^ω at location $x^\omega(t_2^\omega)$, and decelerates with $-a_L$ to speed v_f^ω at the intersection at time t_f^ω.

Travel time $(t_1^\omega - t_0)$ is the root of the following equation:

$$\frac{a_L + a_U}{2a_L} a_U t^2 - \left(t_f^\omega - t_0 + \frac{v_f^\omega - v_0^\omega}{a_L}\right) a_U t + \left(x_0^\omega + \frac{\left(v_0^\omega - v_f^\omega\right)^2}{2a_L} - \left(t_f^\omega - t_0\right) v_0^\omega\right) = 0 \tag{88}$$

As $t_2^\omega \geq t_1^\omega$, it can be proved that $(t_1^\omega - t_0)$ takes the smaller root and t_2^ω is calculated as

$$t_2^\omega = t_f^\omega - \frac{v_0^\omega + a_U\left(t_1^\omega - t_0\right) - v_f^\omega}{a_L} \tag{89}$$

$v^\omega(t_1^\omega)$, $x^\omega(t_1^\omega)$, and $x^\omega(t_2^\omega)$ are calculated as

$$v^\omega(t_1^\omega) = v^\omega(t_2^\omega) = v_0^\omega + a_U(t_1^\omega - t_0) \tag{90}$$

$$x^\omega(t_1^\omega) = x_0^\omega - \frac{v_0^\omega + v^\omega\left(t_1^\omega\right)}{2}(t_1^\omega - t_0) \tag{91}$$

$$x^{\omega}(t_2^{\omega}) = x^{\omega}(t_1^{\omega}) - v^{\omega}(t_1^{\omega})(t_2^{\omega} - t_1^{\omega}) \tag{92}$$

Scenario 3: $\Delta t^{\omega} = \Delta t_{OL}^{\omega}$

Scenario 3–1: $v_0^{\omega} \geq v_f^{\omega}$ ($\Delta t_{OL}^{\omega} = \frac{x_0^{\omega}}{v_0^{\omega}} + \frac{(v_0^{\omega} - v_f^{\omega})^2}{2v_0^{\omega} a_L}$)

Vehicle ω drives with the initial speed v_0^{ω} until time t_1^{ω} at location $x^{\omega}(t_1^{\omega})$, and then decelerates with $-a_L$ to speed v_f^{ω} at the intersection at time t_f^{ω}. Note that if $v_0^{\omega} = v_f^{\omega}$, only the segment with the constant speed exists. t_1^{ω}, $v^{\omega}(t_1^{\omega})$, and $x^{\omega}(t_1^{\omega})$ are calculated as

$$t_1^{\omega} = t_f^{\omega} - \frac{v_0^{\omega} - v_f^{\omega}}{a_L} \tag{93}$$

$$v^{\omega}(t_1^{\omega}) = v_0^{\omega} \tag{94}$$

$$x^{\omega}(t_1^{\omega}) = x_0^{\omega} - v_0^{\omega}(t_1^{\omega} - t_0) \tag{95}$$

Scenario 3–2: $v_0^{\omega} < v_f^{\omega}$ ($\Delta t_{OL}^{\omega} = \frac{x_0^{\omega}}{v_f^{\omega}} + \frac{(v_0^{\omega} - v_f^{\omega})^2}{2v_f^{\omega} a_U}$)

Vehicle ω first accelerates with a_U to speed v_f^{ω} at location $x^{\omega}(t_1^{\omega})$ at time t_1^{ω}, and then drives at the constant speed v_f^{ω} until arriving at the intersection at time t_f^{ω}. t_1^{ω}, $v^{\omega}(t_1^{\omega})$, and $x^{\omega}(t_1^{\omega})$ are calculated as

$$t_1^{\omega} = t_0 + \frac{v_f^{\omega} - v_0^{\omega}}{a_U} \tag{96}$$

$$v^{\omega}(t_1^{\omega}) = v_f^{\omega} \tag{97}$$

$$x^{\omega}(t_1^{\omega}) = x_0^{\omega} - \frac{v_0^{\omega} + v^{\omega}\left(t_1^{\omega}\right)}{2}(t_1^{\omega} - t_0) \tag{98}$$

Scenario 4: $\Delta t_{OL}^{\omega} < \Delta t^{\omega} < \Delta t_{OU}^{\omega}$

The travel time Δt_{OU}^{ω} is calculated as

$$\Delta t_{OU}^{\omega} = \begin{cases} \dfrac{x_0^{\omega}}{v_f^{\omega}} - \dfrac{\left(v_0^{\omega} - v_f^{\omega}\right)^2}{2v_f^{\omega} a_L}, & \text{if } v_0^{\omega} \geq v_f^{\omega} \\ \dfrac{x_0^{\omega}}{v_0^{\omega}} - \dfrac{\left(v_0^{\omega} - v_f^{\omega}\right)^2}{2v_0^{\omega} a_U}, & \text{otherwise} \end{cases} \tag{99}$$

Scenario 4–1: $v_0^{\omega} \geq v_f^{\omega}$ ($\Delta t_{OU}^{\omega} = \frac{x_0^{\omega}}{v_f^{\omega}} - \frac{(v_0^{\omega} - v_f^{\omega})^2}{2v_f^{\omega} a_L}$)

In this scenario, vehicle ω decelerates with $-a_L$ to speed $v^{\omega}(t_1^{\omega})$ at location $x^{\omega}(t_1^{\omega})$ at time t_1^{ω}, maintains the constant speed $v^{\omega}(t_1^{\omega})$ until time t_2^{ω} at location $x^{\omega}(t_2^{\omega})$, and decelerates again to speed v_f^{ω} upon arriving at the intersection at time t_f^{ω}. Note that if $v_0^{\omega} = v_f^{\omega}$, only the segment with the constant speed exists. t_1^{ω}, $v^{\omega}(t_1^{\omega})$, $x^{\omega}(t_1^{\omega})$, t_2^{ω}, $v^{\omega}(t_2^{\omega})$, and $x^{\omega}(t_2^{\omega})$ are calculated as

$$v^{\omega}(t_1^{\omega}) = v^{\omega}(t_2^{\omega}) = \frac{2a_L x_0^{\omega} - \left(v_0^{\omega}\right)^2 + \left(v_f^{\omega}\right)^2}{2\left(a_L\left(t_f^{\omega} - t_0\right) - v_0^{\omega} + v_f^{\omega}\right)} \tag{100}$$

$$t_1^{\omega} = t_0 + \frac{v_0^{\omega} - v^{\omega}\left(t_1^{\omega}\right)}{a_L} \tag{101}$$

$$t_2^{\omega} = t_f^{\omega} - \frac{v^{\omega}\left(t_1^{\omega}\right) - v_f^{\omega}}{a_L} \tag{102}$$

$$x^{\omega}(t_1^{\omega}) = x_0^{\omega} - \frac{v_0^{\omega} + v^{\omega}\left(t_1^{\omega}\right)}{2}(t_1^{\omega} - t_0) \tag{103}$$

$$x^{\omega}(t_2^{\omega}) = x^{\omega}(t_1^{\omega}) - v^{\omega}(t_1^{\omega})(t_2^{\omega} - t_1^{\omega}) \tag{104}$$

Scenario 4–2: $v_0^{\omega} < v_f^{\omega}$ ($\Delta t_{OU}^{\omega} = \frac{x_0^{\omega}}{v_0^{\omega}} - \frac{(v_0^{\omega} - v_f^{\omega})^2}{2v_0^{\omega} a_U}$)

In this scenario, vehicle ω accelerates with a_U to speed $v^\omega(t_1^\omega)$ at location $x^\omega(t_1^\omega)$ at time t_1^ω, maintains the constant speed $v^\omega(t_1^\omega)$ until time t_2^ω at location $x^\omega(t_2^\omega)$, and accelerates again to speed v_f^ω upon arriving at the intersection at time t_f^ω. t_1^ω, $v^\omega(t_1^\omega)$, $x^\omega(t_1^\omega)$, t_2^ω, $v^\omega(t_2^\omega)$, and $x^\omega(t_2^\omega)$ are calculated as

$$v^\omega(t_1^\omega) = v^\omega(t_2^\omega) = \frac{2a_U x_0^\omega + \left(v_0^\omega\right)^2 - \left(v_f^\omega\right)^2}{2\left(a_U\left(t_f^\omega - t_0\right) + v_0^\omega - v_f^\omega\right)} \tag{105}$$

$$t_1^\omega = t_0 + \frac{v^\omega\left(t_1^\omega\right) - v_0^\omega}{a_U} \tag{106}$$

$$t_2^\omega = t_f^\omega - \frac{v_f^\omega - v^\omega\left(t_1^\omega\right)}{a_U} \tag{107}$$

$$x^\omega(t_1^\omega) = x_0^\omega - \frac{v_0^\omega + v^\omega\left(t_1^\omega\right)}{2}(t_1^\omega - t_0) \tag{108}$$

$$x^\omega(t_2^\omega) = x^\omega(t_1^\omega) - v^\omega(t_1^\omega)(t_2^\omega - t_1^\omega) \tag{109}$$

Scenario 5: $\Delta t^\omega = \Delta t_{OU}^\omega$

Scenario 5–1: $v_0^\omega \geq v_f^\omega$ $\left(\Delta t_{OU}^\omega = \frac{x_0^\omega}{v_f^\omega} - \frac{(v_0^\omega - v_f^\omega)^2}{2v_f^\omega a_L}\right)$

In this scenario, vehicle ω first decelerates with $-a_L$ to speed v_f^ω at location $x^\omega(t_1^\omega)$ at time t_1^ω, and then drives at the constant speed v_f^ω until arriving at the intersection at time t_f^ω. Note that if $v_0^\omega = v_f^\omega$, only the segment with the constant speed exists. t_1^ω, $v^\omega(t_1^\omega)$, and $x^\omega(t_1^\omega)$ are calculated as

$$t_1^\omega = t_0 + \frac{v_0^\omega - v_f^\omega}{a_L} \tag{110}$$

$$v^\omega(t_1^\omega) = v_f^\omega \tag{111}$$

$$x^\omega(t_1^\omega) = x_0^\omega - \frac{v_0^\omega + v^\omega\left(t_1^\omega\right)}{2}(t_1^\omega - t_0) \tag{112}$$

Scenario 5–2: $v_0^\omega < v_f^\omega$ $\left(\Delta t_{OU}^\omega = \frac{x_0^\omega}{v_0^\omega} - \frac{(v_0^\omega - v_f^\omega)^2}{2v_0^\omega a_U}\right)$

In this scenario, vehicle ω drives at the initial speed v_0^ω until time t_1^ω at location $x^\omega(t_1^\omega)$, and then accelerates with a_U to speed v_f^ω upon arriving at the intersection at time t_f^ω. t_1^ω, $v^\omega(t_1^\omega)$, and $x^\omega(t_1^\omega)$ are calculated as

$$t_1^\omega = t_f^\omega - \frac{v_f^\omega - v_0^\omega}{a_U} \tag{113}$$

$$v^\omega(t_1^\omega) = v_0^\omega \tag{114}$$

$$x^\omega(t_1^\omega) = x_0^\omega - v_0^\omega(t_1^\omega - t_0) \tag{115}$$

Scenario 6: $\Delta t^\omega > \Delta t_{OU}^\omega$

The travel time Δt_{OU}^ω is calculated in the Eq. (99). In this scenario, vehicle ω decelerates with $-a_L$ to speed $v^\omega(t_1^\omega)$ at location $x^\omega(t_1^\omega)$ at time t_1^ω, maintains this speed until time t_2^ω at location $x^\omega(t_2^\omega)$, and accelerates with a_U to speed v_f^ω upon arriving at the intersection at time t_f^ω.

Travel time $(t_1^\omega - t_0)$ is the root of the following equation:

$$\begin{aligned}&\frac{a_U + a_L}{2a_U}a_L t^2 + \left(\frac{v_{tf} - v_0}{a_U} - \left(t_f^\omega - t_0\right)\right)a_L t \\ &+ \left(v_0^\omega\left(t_f^\omega - t_0\right) + \frac{\left(v_f^\omega - v_0^\omega\right)^2}{2a_U} - x_0^\omega\right) = 0\end{aligned} \tag{116}$$

As $t_2^\omega \geq t_1^\omega$, it can be proved that $(t_1^\omega - t_0)$ takes the smaller root and t_2^ω is calculated as

$$t_2^\omega = t_f^\omega - \frac{v_f^\omega - v_0^\omega + a_L\left(t_1^\omega - t_0\right)}{a_U} \tag{117}$$

$$v^{\omega}(t_1^{\omega}) = v^{\omega}(t_2^{\omega}) = v_0^{\omega} - a_L(t_1^{\omega} - t_0) \tag{118}$$

$$x^{\omega}(t_1^{\omega}) = x_0^{\omega} - \frac{v_0^{\omega} + v^{\omega}\left(t_1^{\omega}\right)}{2}(t_1^{\omega} - t_0) \tag{119}$$

$$x^{\omega}(t_2^{\omega}) = x^{\omega}(t_1^{\omega}) - v^{\omega}(t_1^{\omega})(t_2^{\omega} - t_1^{\omega}) \tag{120}$$

References

Allsop, R.E., 1981. Computer Program Sigset For Calculating Delay-Minimising Traffic Signal Timings – Description and Manual for Users. University College London, Transport Studies Group, London.

Au, T.C., Stone, P., 2010. Motion planning algorithms for autonomous intersection management bridging the gap between task and motion planning. 2010 AAAI Workshops.

Datesh, J., Scherer, W.T., Smith, B.L., 2011. Using K-means clustering to improve traffic signal efficacy in an intellidrive environment. In: 2011 IEEE Forum on Integrated and Sustainable Transportation System (FISTS). IEEE, Vienna, pp. 122–127.

Dresner, K., Stone, P., 2004. Multiagent traffic management: a reservation-based intersection control mechanism. In: Proceedings of the Third International Joint Conference on Autonomous Agents and Multiagent Systems. IEEE Computer Society, New York, pp. 530–537.

Dresner, K., Stone, P., 2007. Sharing the road: autonomous vehicles meet human drivers. In: The 20th International Joint Conference on Artificial Intelligence, pp. 1263–1268.

Dresner, K., Stone, P., 2008. A multiagent approach to autonomous intersection management. J. Artif. Intell. Res. 31, 591–656.

Emmelmann, M., Bochow, B., Kellum, C., 2010. Vehicular Networking: Automotive Applications and Beyond. John Wiley & Sons.

Feng, Y., Head, K.L., Khoshmagham, S., Zamanipour, M., 2015. A real-time adaptive signal control in a connected vehicle environment. Transp. Res. 55, 460–473.

Feng, Y., Yu, C., Liu, H.X., 2018. Spatial and temporal intersection control in a connected and automated vehicle environment. Transp. Res. Part C 89, 364–383.

Frey, H., Unal, A., Chen, J., Li, S., Xuan, C., 2002. Methodology For Developing Modal Emission Rates For Epa's Multi-Scale Motor Vehicle & Equipment Emission System. Ann Arbor, Michigan: US Environmental Protection Agency. North Carolina State University for Office of Transportation and Air Quality, U.S. Environmental Protection Agency, Ann Arbor, MI.

Gurobi Optimization Inc., 2017. Gurobi Optimizer Reference Manual.

He, Q., Head, K.L., Ding, J., 2012. PAMSCOD: platoon-based arterial multi-modal signal control with online data. Transp. Res. Part C 20, 164–184.

He, X., Liu, H.X., Liu, X., 2015. Optimal Vehicle speed trajectory on a signalized arterial with consideration of queue. Transp. Res. Part C 61, 106–120.

Heydecker, B.G., 1992. Sequencing of Traffic Signals. Clarendon Press, Oxford.

Ilgin Guler, S., Menendez, M., Meier, L., 2014. Using connected vehicle technology to improve the efficiency of intersections. Trans. Res. Part C 46, 121–131.

Jiang, H., Hu, J., An, S., Wang, M., Park, B.B., 2017. Eco approaching at an isolated signalized intersection under partially connected and automated vehicles environment. Transp. Res. Part C 79, 290–307.

Kamal, M.A.S., Mukai, M., Murata, J., Kawabe, T., 2013. Model predictive control of vehicles on urban roads for improved fuel economy. IEEE Trans. Control Syst. Technol. 21, 831–841.

Kamalanathsharma, R.K., Rakha, H.A., 2013. Multi-stage dynamic programming algorithm for eco-speed control at traffic signalized intersections. In: 16th International IEEE Conference on Intelligent Transportation Systems (ITSC 2013). IEEE, The Hague, pp. 2094–2099.

Koonce, P., Rodegerdts, L., Lee, K., Quayle, S., Beaird, S., Braud, C., Bonneson, J., Tarnoff, P., Urbanik, T., 2008. Traffic Signal Timing Manual, Final Report ed. Federal Highway Administration, Washington, DC, USA.

Lee, J., Park, B., 2012. Development and evaluation of a cooperative vehicle intersection control algorithm under the connected vehicles environment. IEEE Trans. Intell. Transp. Syst. 13, 81–90.

Li, Z., Elefteriadou, L., Ranka, S., 2014. Signal control optimization for automated vehicles at isolated signalized intersections. Transp. Res. Part C Technol. 49, 1–18.

Malakorn, K.J., Byungkyu, P., 2010. Assessment of mobility, energy, and environment impacts of intellidrive-based cooperative adaptive cruise control and intelligent traffic signal control. In: 2010 IEEE International Symposium on Sustainable Systems and Technology (ISSST). IEEE, Arlington, VA, pp. 1–6.

Marler, R.T., Arora, J.S., 2004. Survey of multi-objective optimization methods for engineering. Struct. Multidiscipl. Optim. 26, 369–395.

Miyatake, M., Kuriyama, M., Takeda, Y., 2011. Theoretical study on eco-driving technique for an electric vehicle considering traffic signals. In: 2011 IEEE Ninth International Conference on Power Electronics and Drive Systems (PEDS), pp. 733–738.

Naidu, D.S., 2002. Optimal Control Systems. CRC Press, Inc., U.S.

National Transportation Operations Coalition (NTOC), 2012. 2012 National Traffic Signal Report Card, Technical Report, Washington, DC.

Newell, G.F., 2002. A simplified car-following theory: a lower order model. Transp. Res. Part B 36, 195–205.

Rakha, H., Kamalanathsharma, R.K., 2011. Eco-driving at signalized intersections using V2i communication. In: 14th International IEEE Conference on Intelligent Transportation Systems (ITSC). IEEE, Washington, DC, pp. 341–346.

Silcock, J.P., 1997. Designing signal-controlled junctions for group-based operation. Transp. Res. Part A 31, 157–173.

Tachet, R., Santi, P., Sobolevsky, S., Reyes-Castro, L.I., Frazzoli, E., Helbing, D., Ratti, C., 2016. Revisiting street intersections using slot-based systems. PLoS ONE 11, 1–9. doi:10.1371/journal.pone.0149607.

Wan, N., Vahidi, A., Luckow, A., 2016. Optimal speed advisory for connected vehicles in arterial roads and the impact on mixed traffic. Transp. Res. Part C 69, 548–563.

Wang, M., Daamen, W., Hoogendoorn, S.P., van Arem, B., 2014a. Rolling horizon control framework for driver assistance systems. part i: mathematical formulation and non-cooperative systems. Transp. Res. Part C 40, 271–289.

Wang, M., Daamen, W., Hoogendoorn, S.P., van Arem, B., 2014b. Rolling horizon control framework for driver assistance systems. part ii: cooperative sensing and cooperative control. Transp. Res. Part C 40, 290–311.

Webster, F.V., 1958. Traffic Signal Settings. Her Majesty's Stationery Office, London, England.

Wong, C.K., Heydecker, B.G., 2011. Optimal allocation of turns to lanes at an isolated signal-controlled junction. Transp. Res. Part B 45, 667–681.

Wong, C.K., Wong, S.C., 2003a. A lane-based optimization method for minimizing delay at isolated signal-controlled junctions. J. Math. Model. Algorithms 2, 379–406.

Wong, C.K., Wong, S.C., 2003b. Lane-based optimization of signal timings for isolated junctions. Transp. Res. Part B 37, 63–84.

Wu, X., He, X., Yu, G., Harmandayan, A., Wang, Y., 2015. Energy-optimal speed control for electric vehicles on signalized arterials. IEEE Transp. Intell. Transp. Syst. 16, 2786–2796.

Yeo, H., Skabardonis, A., Halkias, J., Colyar, J., Alexiadis, V., 2008. Oversaturated freeway flow algorithm for use in next generation simulation. Transp. Res. Record 2088, 68–79.